# A theory of orientation selectivity emerging from randomly sampling the visual field

Wenqing Wei[1,2], Benjamin Merkt[1,2], Stefan Rotter[1,2,*]

**1** Bernstein Center Freiburg, University of Freiburg, 79104 Freiburg, Germany

**2** Faculty of Biology, University of Freiburg, 79104 Freiburg, Germany

* Stefan Rotter, stefan.rotter@bio.uni-freiburg.de

## Abstract

Selectivity for the orientation (OS) of moving gratings is also observed in the primary visual cortex (V1) of species which lack an orientation map, like mice and rats. However, the mechanism underlying the emergence of orientation selectivity in these cases is still mysterious. In the visual pathway, signals from the retina are conveyed to V1 via relay cells in the dorsal lateral geniculate nucleus (dLGN). Here, we explore a computational model of orientation processing in dLGN and V1, where orientation selectivity emerges from random thalamocortical projections and investigate the underlying neuronal mechanism. First we demonstrate that the temporal mean (F0) of the thalamic input to cortical neurons does not depend on orientation, while the amplitude of the temporal modulations (F1) induced by the stimulus grating is indeed tuned to stimulus orientation. Second we show that the orientation tuning in the amplitudes of thalamic input can be transformed into orientation selectivity of V1 neurons by a random network, exploiting the nonlinear input-output transfer function of individual neurons. The untuned excitatory component is largely cancelled by the inhibitory component, such that the operating point is stabilized in the nonlinear regime of the transfer function. In our model, the orientation preference of V1 neurons is sensitive to the spatial frequency of the visual stimulus, very similar to what is found

in neuronal recordings. Finally, we describe a non-linear firing rate model that accounts, among other things, for the F1-to-F0 transfer of oscillatory input to neurons.

## Author summary

Orientation selective neurons are widely observed in mammalian primary visual cortex. Previous theoretical work has argued that contrast-invariant orientation selectivity arises in inhibition-dominated random recurrent networks by attenuating the uninformative component and amplifying a weak orientation bias in the input. Based on a computational model of the thalamocortical pathway, we show that discrete isotropic sampling of the visual field can generate the necessary orientation bias by uneven distribution (random symmetry breaking). This bias is sufficient to induce strong orientation selectivity in a cortical network by exploiting the non-linear transfer of individual neurons. The model exhibits not only biologically plausible behavior of neuronal network, but also suggests a mechanism for the emergence of orientation selectivity in V1. A new firing rate model allows us to determine the output firing rate for oscillatory input without solving the time-dependent Fokker-Planck equation.

## Introduction

Most neurons in the primary visual cortex (V1) of mammals respond selectively to the orientation of light bars, edges of objects, or oriented gratings [1–4]. The phenomenon of orientation selectivity (OS) was first characterized by Hubel and Wiesel in their seminal work [1], and it was since considered as a prototypical example of neural circuit computations. Although a large number of experimental and theoretical approaches have been employed, the exact neuronal mechanisms underlying OS emergence are still controversial. In some mammalian species, neighboring cortical neurons in all layers have a similar orientation preference. The resulting orientation maps on the cortical surface have specifically been described for carnivores [1, 5] and some primates [6, 7]. Despite the absence of smooth orientation maps in other species including rodents, individual V1 neurons still exhibit strong orientation tuning [3, 8, 9]. For that reason, it is not clear that the same exact mechanism of OS emergence applies in all species.

Information about a visual stimulus is mainly conveyed to V1 layer 4 neurons through the relay cells of the dorsal lateral geniculate nucleus (dLGN). In contrast to the elongated receptive fields of V1 neurons, most dLGN cells respond equally to all stimulus orientations and have roughly circular ON/OFF center-surround receptive fields [10]. In the feedforward model originally proposed by Hubel and Wiesel [1], the receptive fields of dLGN neurons converging to a single V1 neuron would be lined up in space. Under certain conditions, this arrangement of inputs would imply an elongated receptive field of the V1 target neuron, which then exhibits selectivity for a stimulus of matching orientation. This simple model, however, cannot explain why orientation tuning depends on the spatial frequency of a grating used for stimulation [11]. In addition, this model requires a mechanism to establish the specific arrangement of receptive fields during development, possibly driven by visual experience. Interestingly, however, mouse V1 neurons exhibit OS already when they open their eyes for the first time and V1 circuits are not yet fully maturated [12]. In this specific case, an alternative mechanism that does not depend on precisely arranged thalamocortical projections might contribute to the emergence of OS. In fact, several alternative mechanisms for OS have been suggested in the past [13].

In previous theoretical work [14–17], it was pointed out that highly selective and contrast-invariant neuronal responses robustly emerge in inhibition-dominated random recurrent networks. Such networks transform a weak orientation bias of the thalamic input into highly selective neuronal responses by attenuating non-informative signal components. In these models, it was assumed that each V1 neuron receives a mix of multiple thalamic inputs with a weak bias for specific orientations. It was, in fact, also reported in experiments that the weak tuning of compound thalamic excitation is amplified by cortical circuits [18], resulting in orientation-specific responses of layer 4 neurons. It remained open, however, where the orientation bias originates and by which mechanism it emerges.

Here we explore the idea that the initial orientation bias might originate from sampling the receptive field at random positions. Provided the number of samples is small, a weak bias emerges by random symmetry breaking, strong enough however to be amplified by the cortical circuit. We demonstrate the feasibility of such a scenario by adopting the inhibition-dominated random network described by Brunel [19] as a model

for V1. The neurons in this network are then fed by convergent inputs from excitatory dLGN neurons, balanced by feedforward inhibition, and exhibit strong contrast-invariant tuning. The dLGN neurons, in turn, receive input from a retina that is activated by a stimulus oriented drifting grating. Consistent with experimental observations [18], we demonstrate that in our model the oscillation amplitude of the random compound dLGN input (F1 component) converging to a single V1 neuron has a weak but significant orientation bias, while the mean (F0 component) is insensitive to stimulus orientation. We then show that the orientation bias in the oscillation amplitude (F1) of the input can be transformed into a tuning for the mean firing rate (F0) of the response, exploiting the non-linear properties of single neurons. Previous computational models also addressed the question whether orientation selective responses can arise from random thalamocortical projections, and how the neuronal responses depend on the spatial properties of the stimulus, as described in experiments [20, 21]. However, these models were so far not able to outline any key neuronal mechanism for these phenomena.

Using numerical simulations, we then investigate the underlying mechanism of OS emergence in the thalamocortical projection. Crucially, the F1-to-F0 transformation, which is the key mechanism of OS emergence in our model, requires a nonlinear transformation. Feedforward inhibition is introduced in the network model to compensate for the excitatory thalamic input and stabilize the operating point of the network in the nonlinear regime. Resulting from this nonlinear input-output transformation, orientation selective V1 neurons can be obtained from random TC connectivity. Furthermore, orientation selectivity in the network depends on the number of convergent thalamic inputs, as well as the spatial frequency of the grating used for stimulation. In our work, we not only propose a thalamocortical network model where orientation selectivity emerges naturally from a random configuration of dLGN neurons, but can also investigate the mechanism underlying it. This nonlinear input-output transformation might also provide new insight into computations in other sensory systems that rely on the processing of oscillatory signals.

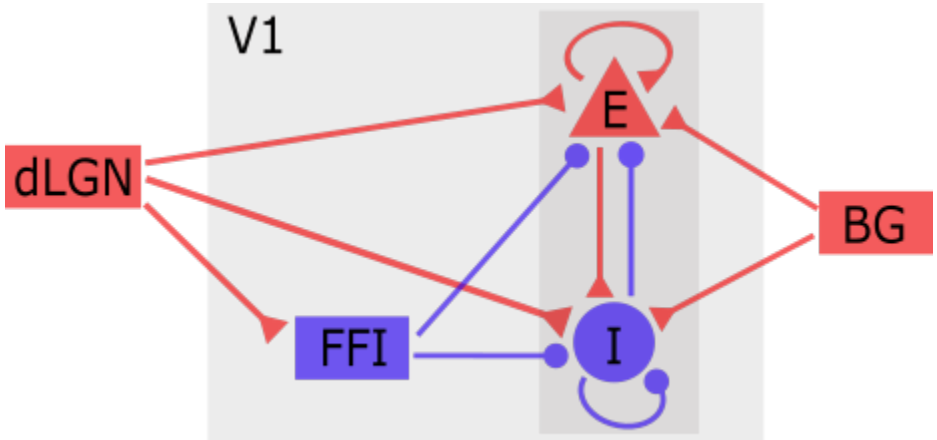


**Fig 1. Configuration of the thalamocortical network model.** The primary visual cortex (V1) comprises different types of excitatory (red) and inhibitory (blue) neurons. The thalamus (dLGN) relays light-induced activity of the retina to V1. Unspecific background input (BG) provides additional excitatory drive independent of the stimulus. Stimulus processing is collectively performed by all V1 neurons. Feedforward inhibition (FFI) and recurrent inhibition (I) together balance the recurrent excitation (E) of cortical pyramidal neurons and stabilize the operating point of the network.

# Materials and methods

## Description of the model system

### Network model

The basic model network used in this work is composed of two parts: the thalamic (dLGN) feedforward projection and the cortical (V1) recurrent network (Fig 1). The layout of our V1 network is identical to the one introduced by Nicolas Brunel [19]. It consists of $N = 12\,500$ leaky integrate-and-fire neurons, of which $a = 80\%$ are excitatory and $1 - a = 20\%$ are inhibitory. The recurrent connectivity $\epsilon = 10\%$ is uniform throughout the network [22]. As a result, each neuron receives exactly 1 000 excitatory and 250 inhibitory inputs from within the same network, drawn randomly and independently. Self-connections are excluded. The amplitudes of excitatory recurrent synapses are $J_{\mathrm{E}} = 0.2\,\mathrm{mV}$. Inhibitory couplings are set to be $g = 8$ times stronger than excitatory ones. As a consequence, the amplitudes of inhibitory synapses are $J_{\mathrm{I}} = -gJ_{\mathrm{E}} = -1.6\,\mathrm{mV}$. This results in an inhibition-dominated recurrent network.

Besides recurrent input, V1 neurons receive additional feedforward input from three sources: constant background, thalamic excitation and feedforward inhibition.

Background inputs represent projections from any other brain areas except visual thalamus. In our model, they are identical for all recurrent neurons and keep the recurrent neural activity going in absence of visual stimulation. They are rendered as a stationary Poisson process with constant rate $\nu_{\mathrm{bg}}$. The synaptic weights are $J_{\mathrm{bg}} = 0.1\,\mathrm{mV}$ for all simulations. The second input source is the visual thalamus. In the primary visual cortex, the visual information is mainly conveyed by the dorsal lateral geniculate nucleus (dLGN) through thalamocortical projections. A recurrent V1 neuron receives input from exactly $K_{\mathrm{V1}}^{\mathrm{dLGN}}$ neurons in dLGN. As a result, the emerging receptive fields of recurrent V1 neurons are of similar size, but vary slightly from neuron to neuron. Receptive fields are roughly circular, but non-uniform, reflecting the random positions of dLGN inputs. Experiments *in vitro* reported that thalamocortical synapses are several times stronger than intracortical synapses [23, 24]. Here, we assume that the efficacy of direct thalamocortical projections is 10 times larger than recurrent excitatory connections, $J_{\mathrm{V1}}^{\mathrm{dLGN}} = 2.0\,\mathrm{mV}$. The third source of input are feedforward inhibitory projections (FFI) from other cortical neurons. FFI neurons represent a specific type of inhibitory interneurons, which selectively target recurrent V1 neurons. They receive input from $K_{\mathrm{FFI}}^{\mathrm{dLGN}}$ neurons in dLGN, each with a synaptic efficacy of $J_{\mathrm{FFI}}^{\mathrm{dLGN}}$. Thalamic afferents are the only driver of FFI neurons in our model, so their activity is fully determined by its thalamic inputs. Finally, $K_{\mathrm{V1}}^{\mathrm{FFI}}$ FFI neurons project onto each V1 neuron, each with synaptic weight $J_{\mathrm{V1}}^{\mathrm{FFI}}$. In the cortical circuit just described, the connections between FFI neurons and recurrent V1 neurons are established randomly and independently.

### Neurons and receptive fields

Neurons in the lateral geniculate nucleus (dLGN) have circular antagonistic center-surround receptive fields, either ON-center/OFF-surround or OFF-center/ON-surround. ON-center cells respond strongest when the center of their receptive fields is exposed to light, and they are inhibited when the surround is illuminated. OFF-center cells respond in exactly the opposite way. The center and surround sub-regions of the receptive field are described by two-dimensional normalized Gaussian functions of different widths $\sigma_+$ and $\sigma_-$, respectively. For ON-center cells, we have $\sigma_+ < \sigma_-$ and $\sigma_+ > \sigma_-$ for OFF-center cells. The receptive field is simply

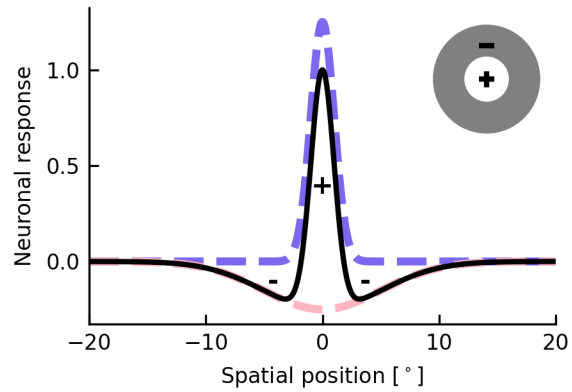


**Fig 2. Isotropic receptive field of dLGN neurons.** The two-dimensional receptive field of a single dLGN neuron is conceived as difference of Gaussians (DOG). Shown is the neuronal response (solid line) of an ON-center/OFF-surround cell (inset) to small spots of light at the position indicated. Dashed lines represent the responses for a separate stimulation of either the center or the surround, respectively.

represented by the difference of these two Gaussians (DoG), respectively. Fig 2 shows an example of the receptive field of an ON-center cell. In our model, an equal number of ON-center and OFF-center cells are distributed randomly in the visual field.

In order to investigate orientation selectivity in line with experiments, we use moving oriented gratings with luminance changing sinusoidally both in space and time. Each of these visual stimuli has an orientation $\theta$, a temporal frequency $f$ and a spatial frequency $\lambda$. The movement direction of the grating is always orthogonal to its orientation. The light intensity of the stimulus at position $(x, y)$ at time $t$ is given by

$$S(x, y, t) = s_0[1 + C\cos(k \cdot (x, y) - 2\pi f t)] \tag{1}$$

where $k = 2\pi\lambda(\sin(\theta), -\cos(\theta))$ is the wave vector, $s_0$ the mean luminance of the stimulus and $C$ the contrast of the grating. The resulting firing rate of dLGN neuron $i$ at position $(x_i, y_i)$ in response to the stimulus grating can then be calculated as

$$\nu_i(t) = \nu_b + C\nu_0 m \cos\left(k \cdot (x_i, y_i) - 2\pi f t\right) \tag{2}$$

where $m = e^{-\frac{(2\pi\lambda\sigma_+)^2}{2}} - e^{-\frac{(2\pi\lambda\sigma_-)^2}{2}}$ and $\nu_0$ is the rate of a dLGN neuron in response to the mean stimulus luminance $s_0$. $m_{\max}$ is the maximum value of $m$ for a given set of $(\sigma_+, \sigma_-)$ when varying the spatial frequency $\lambda$. The baseline firing rate is given by

$\nu_b = m_{\max}\nu_0$ such that the firing rate of a single dLGN neuron will always be non-negative.

The dLGN neurons are modeled as Poisson neurons, i.e. spikes are generated randomly and independently with firing rate $\nu_i(t)$ at each point in time. A Dirac delta-function $\delta(t - t_i^k)$ is used to represent spike $k$ generated by neuron $i$. The spike train of dLGN neuron $i$ is the sum of all spikes it generates $\sum_k \delta(t - t_i^k)$.

Cortical neurons, in contrast, are conceived as leaky integrate-and-fire (LIF) neurons. The sub-threshold time evolution of the membrane potential $V_i(t)$ of neuron $i$ is determined by

$$\tau_m \dot{V}_i(t) + [V_i(t) - V_\mathrm{r}] = R I_i(t)\,, \tag{3}$$

where $\tau_m$ is the membrane time constant and $R$ is the leak resistance. The current $I_i(t)$ represents the total input to neuron $i$. A spike is elicited when the membrane potential reaches the threshold $V_\mathrm{th}$, after which $V_i(t)$ is reset to its resting potential $V_\mathrm{r}$. It remains at the resting potential for a short refractory period $t_\mathrm{ref}$. During this absolute refractory period, no spike will be generated.

## Mathematical implementation of the model

### Network of spiking neurons

In order to study the orientation preference of recurrent neurons in the network described above, we set up a spiking neuronal network. In this network, cortical neurons receive presynaptic spike inputs, resulting in transient changes of the postsynaptic membrane potential. Excitatory and inhibitory recurrent neurons, as well as FFI neurons, are conceived as leaky integrate-and-fire neurons. The time evolution of the membrane potential $V_i(t)$ is described by a differential equation Eq 3, separately for each neuron $i$. Thereby, the total input current $I_i(t)$ is the superposition of all inputs

$$I_i(t) = I_i^\mathrm{rec} + I_i^\mathrm{bg} + I_i^\mathrm{dLGN} + I_i^\mathrm{FFI}\,, \tag{4}$$

accounting for their respective synaptic strengths.

The background inputs $I_i^\mathrm{bg}$ are all identical and target recurrent V1 neurons. They are modeled as a Poisson process with mean firing rate $\nu_\mathrm{bg}$. The corresponding

background input current is given by

$$RI_i^{\mathrm{bg}}(t) = \tau_m J_{\mathrm{bg}} \sum_k \delta(t - t^k - D)\,, \tag{5}$$

where $t^k$ is the emission time of $k$-th spike of the input and $J_{bg}$ is the amplitude of postsynaptic potential.

In all other pathways, convergent projections need to be accounted for. Therefore, the input current of each component is given by the sum of spike input from all presynaptic neurons, indexed by $j$

$$\begin{aligned} RI_i^{\mathrm{rec}}(t) &= \tau_m \sum_j J_{ij} \sum_k \delta(t_j^k + D - t) \\ RI_i^{\mathrm{dLGN}}(t) &= \tau_m \sum_j J_{\mathrm{V1}}^{\mathrm{dLGN}} \sum_k \delta(t_j^k + D - t) \\ RI_i^{\mathrm{FFI}}(t) &= \tau_m \sum_j J_{\mathrm{V1}}^{\mathrm{FFI}} \sum_k \delta(t_j^k + D - t)\,. \end{aligned} \tag{6}$$

Note that this entails $\epsilon N$, $K_{\mathrm{V1}}^{\mathrm{dLGN}}$ and $K_{\mathrm{V1}}^{\mathrm{FFI}}$ non-zero contributions to the respective sum, respectively. Although the convergence numbers are the same for all recurrent V1 neurons in each pathway, their presynaptic neurons are different. As the FFI neurons are also modeled as LIF neurons, the same method was be applied to calculate their input currents and then extract the respective spike trains.

Combining all the inputs above, the V1 neurons in the network respond to a visual stimulus in terms of spike trains. All numerical simulations of this model were performed in the neural simulation tool NEST [25, 26]. All the parameters used in numerical simulations are shown in Table 1.

### Analytical firing rate model

Although spiking neurons (here, LIF) provide a more biologically realistic model, the numerical effort to study input-output transfer functions via simulations is quite high. To reduce the effort, and to provide additional mathematical insight, we employed analytical firing rate models that generalize the well-known diffusion approximation to certain time-dependent inputs. First, we devised a stationary rate model (SRM) to estimate the output. Assuming that the input to the neuron changes slowly, allowing

that it is in equilibrium in every moment, we can just use the known steady-state solution, moment by moment. However, this approach has limitations. As in the setting considered here V1 neurons receive oscillatory inputs from the thalamus, a dynamic rate model (DRM) appeared to be more appropriate. As the membrane acts as a lowpass with frequency-dependent attenuation, we assume that the input amplitude depends on the temporal frequency $f$ according to $\frac{1}{\sqrt{1+(2\pi\tau f)^2}}$, where $\tau$ is the time constant of the membrane. On this basis, the DRM provides good estimates of the output firing rate for a wider range of temporal frequencies.

The nonlinear firing rate model used here is based on the diffusion approximation to single neurons, see e.g. [19, 27–29]. In this setting, the total synaptic input current to a neuron $i$ is replaced by a Gaussian White Noise of mean $\mu_i$ and amplitude $\sigma_i$, which drives the neuron in an equivalent way

$$RI_i(t) = \mu_i(t) + \sigma_i\sqrt{\tau_m}\eta_i(t)\,, \tag{7}$$

As described above, the total input to a single recurrent V1 neuron is composed of the recurrent and feedforward inputs from four sources. Assuming their statistical independence, this yields

$$\begin{aligned} \mu_i(t) &= \mu_i^{\mathrm{rec}} + \mu_i^{\mathrm{bg}} + \mu_i^{\mathrm{dLGN}} + \mu_i^{\mathrm{FFI}} \\ \sigma_i^2(t) &= \sigma_i^{\mathrm{rec}^2} + \sigma_i^{\mathrm{bg}^2} + \sigma_i^{\mathrm{dLGN}^2} + \sigma_i^{\mathrm{FFI}^2}\,. \end{aligned} \tag{8}$$

Mean and variance of each source is related to the respective presynaptic firing rates $\nu$ and synaptic strength $J$. When a sinusoidal grating moves over the visual field, the firing rates of all individual dLGN neurons change sinusoidally over time (see Eq 2). As the rate of background input is fixed for all recurrent V1 neurons, the mean and variance of the background input is constant over time. The rates of FFI neurons are determined

by their thalamic inputs. The mean and variance of each part is then given by

$$
\begin{aligned}
\mu_i^{\mathrm{rec}}(t) &= \tau_m \sum_{j=1} J_{ij}\nu_j(t), & \sigma_i^{\mathrm{rec}^2}(t) &= \tau_m \sum_{j=1} J_{ij}^2\nu_j(t) \\
\mu_i^{\mathrm{bg}} &= \tau_m J_{\mathrm{bg}}\nu^{\mathrm{bg}}, & \sigma_i^{\mathrm{bg}^2} &= \tau_m J_{\mathrm{bg}}^2\nu^{\mathrm{bg}} \\
\mu_i^{\mathrm{dLGN}}(t) &= \tau_m \sum_{j=1} J_{\mathrm{V1}}^{\mathrm{dLGN}}\nu_j^{\mathrm{dLGN}}(t), & \sigma_i^{\mathrm{dLGN}^2}(t) &= \tau_m \sum_{j=1} J_{\mathrm{V1}}^{\mathrm{dLGN}^2}\nu_j^{\mathrm{dLGN}}(t) \\
\mu_i^{\mathrm{FFI}}(t) &= \tau_m \sum_{j=1} J_{\mathrm{V1}}^{\mathrm{FFI}}\nu_j^{\mathrm{FFI}}(t), & \sigma_i^{\mathrm{FFI}^2}(t) &= \tau_m \sum_{j=1} J_{\mathrm{V1}}^{\mathrm{FFI}^2}\nu_j^{\mathrm{FFI}}(t)\,.
\end{aligned}
\tag{9}
$$

The steady-state firing rate of all recurrent V1 neurons are given by a transfer function $F_i$ [27]

$$
\nu_i = F_i(\nu, \nu_i^{\mathrm{dLGN}}, \nu_i^{\mathrm{FFI}})\,, \tag{10}
$$

where $F_i$ is defined by

$$
F_i(\nu, \nu_i^{\mathrm{dLGN}}, \nu_i^{\mathrm{FFI}}) = \left[\tau_{\mathrm{ref}} + \tau_m\sqrt{\pi}\int_{\frac{V_{\mathrm{r}}-\mu_i}{\sigma_i}}^{\frac{V_{\mathrm{th}}-\mu_i}{\sigma_i}} e^{x^2}(1+\mathrm{erf}(x))\,dx\right]^{-1} \tag{11}
$$

where erf is the error function. The self-consistent solutions of these nonlinear equations will return the estimation of the firing rates of individual recurrent neurons.

The firing rates of FFI neurons are easier to obtain, as there are no recurrent connections and we do not need to solve the equations self-consistently. As each FFI neuron $i$ only receives inputs from dLGN neurons, its input mean and variance is given by

$$
\begin{aligned}
\mu_i(t) = \mu_i^{\mathrm{dLGN}}(t) &= \tau_m \sum_{j=1} J_{\mathrm{FFI}}^{\mathrm{dLGN}}\nu_j^{\mathrm{dLGN}}(t) \\
\sigma_i^2 = \sigma_i^{\mathrm{dLGN}^2} &= \tau_m \sum_{j=1} J_{\mathrm{FFI}}^{\mathrm{dLGN}^2}\nu_j^{\mathrm{dLGN}}(t)\,.
\end{aligned}
\tag{12}
$$

The steady state firing rate of FFI neuron $i$ can be calculated from the transfer function $F_i(\nu_i^{\mathrm{dLGN}})$ by solving Eq 11 with their respective inputs.

## Data analysis

### Orientation selectivity

To quantify the orientation selectivity of single cortical neurons, the preferred orientation (PO) and the orientation selectivity index (OSI) are calculated for each neuron. This information can be extracted from its respective tuning curve, $\nu(\theta)$, representing the mean firing rate of a neuron for stimulus orientation $\theta$. The method used here is to first compute the orientation selectivity "vector" (here represented as a complex number) [30, 31]

$$\overrightarrow{\mathrm{OSV}} = \frac{\sum_\theta \nu(\theta) e^{2i\theta}}{\sum_\theta \nu(\theta)} \,. \tag{13}$$

The PO is then extracted as the phase (angle) of the OSV

$$\mathrm{PO} = \arg(\overrightarrow{\mathrm{OSV}}) \,. \tag{14}$$

In contrast, the OSI is extracted as the magnitude (length) of the OSV

$$\mathrm{OSI} = |\overrightarrow{\mathrm{OSV}}| \,. \tag{15}$$

The OSI is often used to describe the strength of orientation selectivity. A neuron with high orientation selectivity, which only responds to one stimulus orientation and keeps silent for other orientations, returns $\mathrm{OSI} = 1$. For an unselective neuron responding to all orientations equally, we have $\mathrm{OSI} = 0$.

In some experimental literature, an alternative measure of orientation selectivity is used. It is calculated by $\mathrm{OSI}^* = (\nu_{\mathrm{pref}} - \nu_{\mathrm{orth}})/(\nu_{\mathrm{pref}} + \nu_{\mathrm{orth}})$, where $\nu_{\mathrm{pref}}$ is the firing rate at the preferred orientation and $\nu_{\mathrm{orth}}$ is the firing rate at its orthogonal orientation. In previous theoretical work, it has been pointed out that, for a perfect cosine tuning curve, $\mathrm{OSI}^*$ is twice as large as the OSI [16].

### Preferred orientation

In order to evaluate the comparison of the orientation preference across different conditions (e.g. spatial frequency of the stimulus), we use the circular correlation (CC) of PO [21]. If $\mathrm{PO}_i$ is the preferred orientation of neuron $i$ at one spatial frequency,

$\theta_{ij} = \mathrm{PO}_i - \mathrm{PO}_j$ is the difference of PO of neuron $i$ and $j$ at this spatial frequency, and $\theta'_{ij}$ is the difference of neuron $i$ and $j$ at another spatial frequency. The circular correlation between PO at different spatial frequencies is extracted by

$$\mathrm{CC}(\theta_{ij}, \theta'_{ij}) = \frac{\sum_{i,j} \sin(\theta_{ij}) \sin(\theta'_{ij})}{\sqrt{\sum_{i,j} \sin^2(\theta_{ij}) \sum_{i,j} \sin^2(\theta'_{ij})}} \,. \tag{16}$$

The value of CC ranges from $-1$ to 1. The preferred orientations at different spatial frequencies are perfectly linear correlated when $\mathrm{CC} = 1$, and $\mathrm{CC} = 0$ means no correlation between them.

### Receptive fields

The receptive fields of cortical recurrent neurons and their respective thalamic inputs are mapped using locally sparse noise (Fig S1). For each stimulus image, an equal number of white and black spots are placed randomly in the visual field on the gray background matching the mean luminance at the mean input. Around 20% of the visual field is filled with spots. In order to eliminate boundary effects of dLGN neurons at the border of the visual field, the stimulus image is extended with gray background . The diameter of the spots is 4° so that it is roughly the same as the center size of dLGN receptive fields. 20 000 stimulus frames are used during simulation and each frame is presented for 33 ms. Receptive fields are then estimated by reverse correlation. It is a commonly used method to reconstruct the receptive fields by averaging all the frames, each of them weighted by the response that it evoked [32]. Note that no extra smoothing was applied to the figures of receptive fields.

## Results

Can orientation selective neuronal responses in the primary visual cortex emerge from random thalamocortical projections? To address the feasibility of such a scenario and identify the underlying neuronal circuit mechanisms, we performed numerical simulations of a thalamocortical network model, using sinusoidal drifting gratings for visual stimulation (cf. Eq 1). The stimuli were presented at 12 different orientations, uniformly sampling all orientations between 0° and 180° in discrete steps of 15°. The

movement direction was always orthogonal to the orientation of the grating.

## Orientation tuning of compound thalamic activity

In our model, neurons in the dLGN are assumed to have circular receptive fields. The activity induced by a grating passing by is an oscillation with the temporal frequency of the grating (cf. Eq 2). Information about the orientation of the stimulus lies only in the phase of the oscillatory activation. Neither the temporal mean, nor the oscillation amplitude of single neuron activity is sensitive for the orientation of the stimulus. The actual input to cortical neurons, however, comes from multiple thalamic neurons. Here we assume that each cortical neuron receives the same number $K_{\mathrm{V1}}^{\mathrm{dLGN}}$ of thalamic inputs. The compound signal is again a harmonic oscillation of the same frequency, but the phases of its components matter. Depending on the relative positions of all contributing dLGN neurons, the oscillation amplitude of the compound signal may now be tuned to the orientation of the grating.

The compound thalamic input to a single V1 neuron $i$ is a linear sum of the responses of all presynaptic neurons

$$\begin{aligned} \nu_i^{\mathrm{dLGN}}(t) &= \sum_{j=1}^{K_{\mathrm{V1}}^{\mathrm{dLGN}}} \nu_j(t) \\ &= \sum_{j=1}^{K_{\mathrm{V1}}^{\mathrm{dLGN}}} \nu_b + \sum_{j=1}^{K_{\mathrm{V1}}^{\mathrm{dLGN}}} C \cdot \nu_0 m \cos\left[k \cdot (x_i, y_i) - 2\pi f t)\right]. \end{aligned} \tag{17}$$

The compound signal is again a sine function. Its mean (F0 component) and its amplitude (F1 component) can be calculated using the Fourier theorem [33]

$$\begin{aligned} \mathrm{F0}_i &= \left\langle \nu_i^{\mathrm{dLGN}}(t) \right\rangle = K_{\mathrm{V1}}^{\mathrm{dLGN}} \nu_b \\ \mathrm{F1}_i &= C \cdot \nu_0 m \sqrt{K_{\mathrm{V1}}^{\mathrm{dLGN}} + 2 \sum_{\substack{j,k=1 \\ j \neq k}}^{n} \cos(\alpha_j - \alpha_k)} \end{aligned} \tag{18}$$

where $\alpha_j = k \cdot (x_j, y_j)$ with $k$ determined by the stimulus orientation $\theta$ and spatial frequency $\lambda$ (see Materials and methods).

In our model, the receptive field centers of dLGN neurons are randomly positioned, assuming a uniform coverage of the visual field. Each V1 neuron receives input from

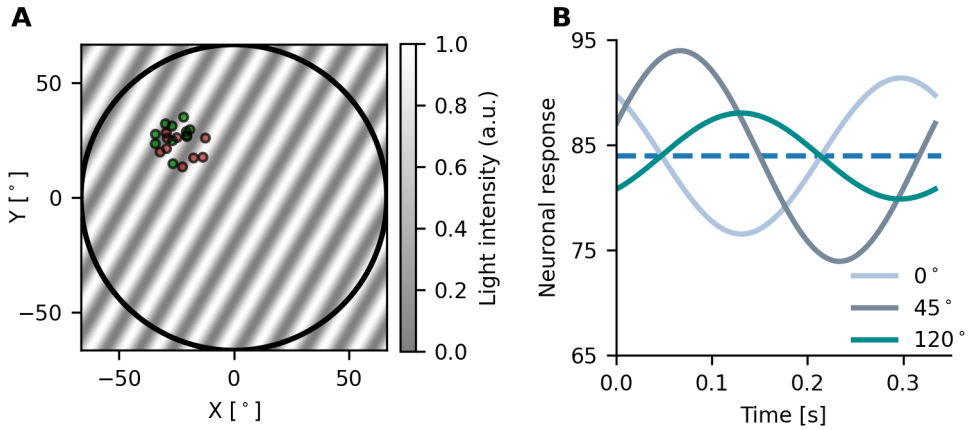


**Fig 3. Compound thalamic input to the cortex. A** In the example shown here, each cortical neuron receives input from 100 dLGN neurons. The receptive field of each dLGN neuron is indicated by a circle, shown are 20 out of 100 receptive fields. Red and blue circles denote ON and OFF center receptive fields, respectively. Receptive field centers are randomly distributed and uniformly cover the (larger) receptive field of the target V1 neuron. The background shows a stimulus grating with an orientation of 60° and a spatial frequency of 0.08 cycles per degree (cpd). **B** Not only the activity of individual dLGN neurons, but also the compound signal of a group of dLGN neurons reflect the temporal modulation induced by a drifting grating. Solid lines of different colors correspond to the temporal responses for different orientations of the grating, respectively. The dashed line indicates the temporal mean of the compound signal, which does not depend on stimulus orientation.

those dLGN neurons whose receptive fields are closest to the receptive field center. As a result, the receptive fields of V1 neurons are not all of the same size, although the number of inputs is the same (see Fig 3). The receptive fields of both ON center and OFF center dLGN cells are randomly positioned within the receptive field of their target V1 neuron. Fig 3B shows the temporal profiles of the compound input signal for different stimulus orientations. Importantly, the mean (F0 component) does not depend on the orientation, while the amplitude (F1 component) is significantly tuned to orientation. In agreement with this result, it was also shown in experiments [18] that it is mainly the F1 component of thalamic excitation that is tuned to stimulus orientation.

## Nonlinear signal transmission of single LIF neurons

We have demonstrated that the oscillation amplitude of thalamic compound input to cortical neurons is tuned to stimulus orientation. As the temporal mean of the compound input is essentially untuned, it is necessary to explain how information about orientation in the input is transformed to a tuned spike response of the neuron. To

derive a quantitative description of this transformation, we assume that a LIF neuron receives effective excitatory and inhibitory input matching the input level in our network simulation. The compound excitatory input is again a cosine wave, and the inhibitory input is constant. Therefore, the effective input to the LIF neuron is characterized by a baseline and by the amplitude of the cosine, its phase is irrelevant for the questions discussed here. As the input is realized as a Poissonian barrage of action potentials with time-varying rate, we have an effective description of the resulting postsynaptic current as Gaussian White Noise with a mean $\mu_t$ and a fluctuation amplitude $\sigma_t$ that depends on the input rates [19]. We assume that the neuron is always at its steady state, producing an output that follows a slow temporal modulation of its input. Its instantaneous firing rate $\nu_t$ is then given by the nonlinear transfer function

$$\nu_t = \left[\tau_{\mathrm{ref}} + \tau_m \sqrt{\pi} \int_{\frac{V_{\mathrm{r}}-\mu_t}{\sigma_t}}^{\frac{V_{\mathrm{th}}-\mu_t}{\sigma_t}} e^{x^2} (1 + \mathrm{erf}(x))\, dx\right]^{-1}, \tag{19}$$

where the parameters $\tau_m$, $V_{\mathrm{th}}$ and $V_{\mathrm{r}}$ characterize the neuron biophysically. The mean response rate of the neuron is conceived as the temporal mean of $\nu_t$. As the instantaneous firing rate $\nu_t$ has the same period as the cosine input, it is sufficient to average over one oscillation period to obtain the temporal mean (see Fig 4). It is obvious that the mean of the temporal input (Fig 4A1) does not meet the mean of the output (Fig 4A3) on the nonlinear transfer curve (Fig 4A2). This means that the input mean is not the only factor that contributes to the output mean. When the operating point is in the nonlinear regime, the oscillatory input curve is distorted by the transfer curve and the input amplitude is also a determinant factor of the degree of distortion. The stationary rate model (SRM) adopted here is normally used to describe the input-output relation of a LIF neuron for stationary Poisson input. As here the input is not stationary, however, we have to additionally account for the lowpass filter properties of the postsynaptic membrane. This motivates the dynamic rate model (DRM) adopted here. Since the excitatory input is oscillatory, its amplitude is attenuated by the frequency-dependent factor $\frac{1}{\sqrt{1+(2\pi\tau f)^2}}$ that can be derived by Fourier transforming the leaky integrator equation for the subthreshold response of the neuronal membrane. We compared the output firing rates of both rate models and the simulated LIF model (SIM) for different temporal frequencies. We generally found a good agreement between

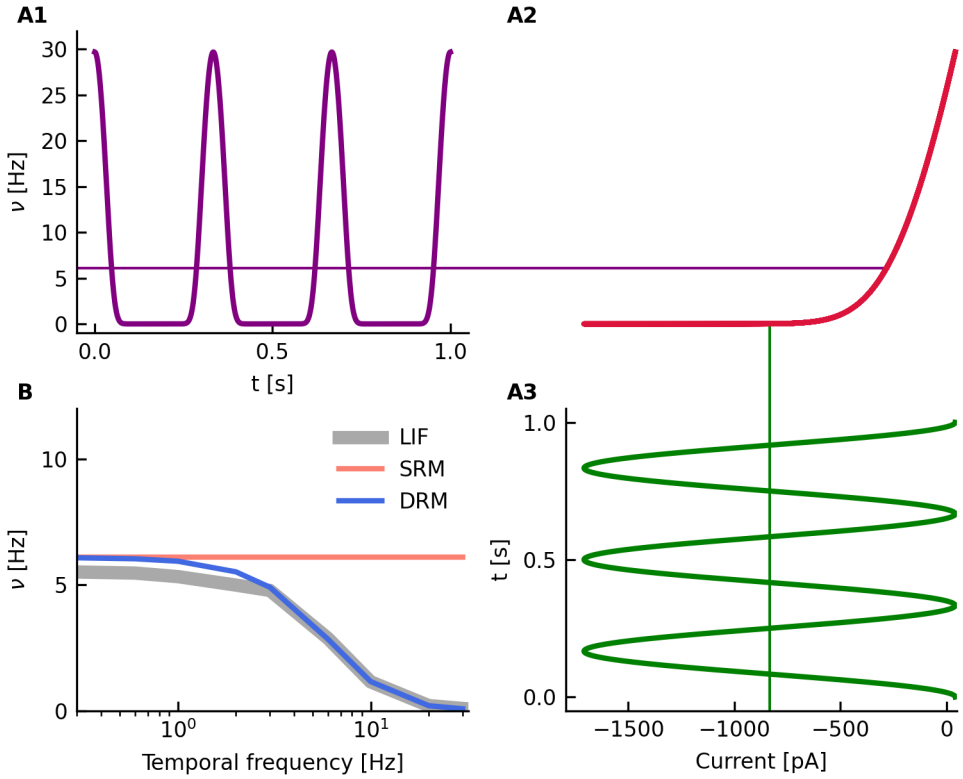


**Fig 4. Nonlinear signal transmission of single neurons. A1** Time-dependent output firing rate of a single spiking neuron (LIF) during stimulation with a drifting grating. Thin lines indicate the temporal mean of the time-dependent signal of the same color. The temporal frequency of the grating is 3 Hz. **A2** The input-output transfer function of the sample neuron shown. The output firing rate is scattered against the input current. **A3** Time-dependent current input to the LIF neuron, induced by a drifting grating. As a superposition of sine-waves with a common frequency it also changes sinusoidally over time. **B** Comparison of single neuron firing rates of three different model neurons, for different temporal frequencies: numerical simulation of a spiking neuron (LIF), static rate model (SRM), dynamic rate model (DRM).

SRM and SIM at low frequencies and a significant discrepancy at higher frequencies. The DRM, in contrast, fits well to the SIM for all temporal frequencies (Fig 4).

The simulation of a LIF neuron reveals a specific dependence of the output rate on both the baseline and the amplitude of the input. Therefore, we investigate the effects of changing baseline and amplitude separately. When the baseline of the input is fixed and the amplitude increases (Fig 5A), the output firing rate also gets larger (Fig 5B). Observe that the mean output firing rate varies nonlinearly with input amplitude (Fig 5C). A similar nonlinear dependency is obtained when fixing the amplitude and changing the baseline of the input (Fig 5D-F). Altogether, this implies that the output

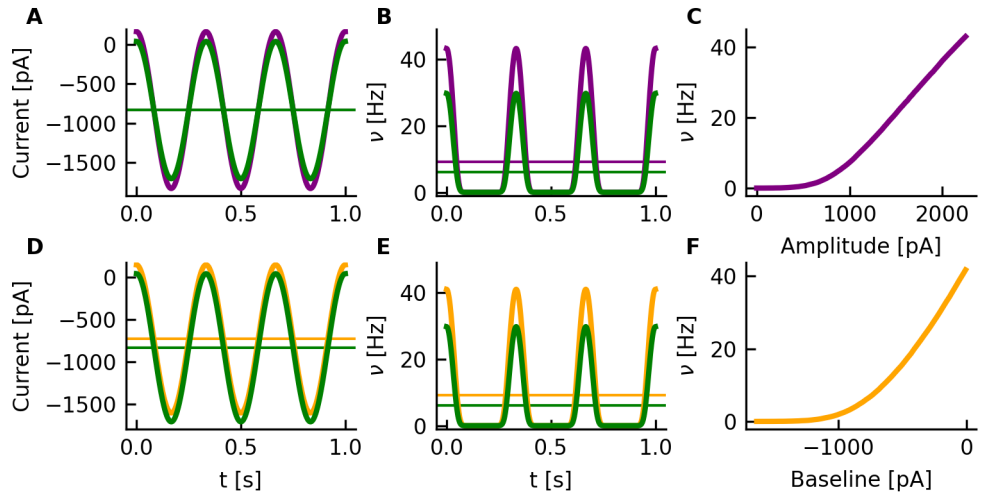


**Fig 5. Nonlinear transduction of oscillatory input to a neuron. A** The input current to a LIF neuron is a harmonic oscillation with a certain amplitude and additive offset. The green signal is the same as in Fig 4A3. The purple signal represents an oscillation with a larger amplitude, but the same baseline. Thin horizontal lines indicate the temporal mean of the signal with matching color. **B** Time-dependent output rate of the LIF neuron (see text for parameters), obtained by numerical simulation. Note the nonlinear distortion of the harmonic oscillation offered as input. **C** The amplitude of the input current is nonlinearly transformed to the mean output rate, assuming a fixed baseline. **D-F** Orange color indicates the outcome of a changing baseline and fixed amplitude.

of a single neuron depends on the baseline and the amplitude of the input in a nonlinear fashion.

## Orientation selectivity emerges from random TC projections

In previous sections, firstly, we found that the compound signal of a random sample of thalamic neurons has an orientation bias. Secondly, we showed a nonlinear dependence of a single neuron on the F0 and F1 components of the input. In combine with these two findings, we now address the question how tuning in the amplitude of compound thalamic input to cortical neurons could be transformed to tuned firing rates. To this end, we devise a thalamo-cortical network model (Fig 1) and perform computer simulations of its activity dynamics. The network model of V1 has been described by Sadeh et al. [16], based on seminal work by Brunel [19]. The V1 network model consists of $N = 12\,500$ leaky integrate-and-fire (LIF) neurons, of which 80% are excitatory and 20% are inhibitory. Each V1 neuron receives input from $\epsilon = 10\%$ of all excitatory and inhibitory neurons, the connectivity is random. Inhibitory synapses are $g = 8$ times

stronger than excitatory synapses, resulting in an inhibition dominated network. A new feature of the model considered here is the feedforward inhibition (FFI), which effectively provides inhibitory thalamic input on top of the direct excitatory dLGN input. Each neuron in the recurrent network receives the same constant background input, which helps adjusting the operating point and also sets the mean response rate. All spiking network simulations are performed in NEST [26].

In order to investigate the orientation preference of V1 neurons, we stimulate the thalamo-cortical network with sinusoidal moving gratings at 12 different orientations evenly distributed between 0° and 180°. Then, the tuning curves of individual recurrent V1 neurons are extracted from the recorded spike trains. To evaluate orientation preference quantitatively and study its dependence on the input, we calculate the preferred orientation (PO) and the orientation selectivity index (OSI) from the tuning curves, using circular statistics. The PO is an angle between 0° and 180°. The OSI is a number between 0 and 1, where higher values denote a more pronounced orientation selectivity. First, we seek to find out which component of the compound thalamic input conveys the orientation bias. The thalamic input of a randomly selected cortical neuron is depicted in Fig 6, along with some important analysis results. The input current is quite noisy, as a result of the random arrival of spikes generated by thalamic neurons. Fourier transformation yields that the F0 and F1 components together carry most of the signal power. The orientation bias, however, selectively shows up in the F1 component of the compound thalamic input.

The total feedforward input to recurrent cortical neurons is composed of time-dependent excitation from dLGN neurons, inhibition from cortical FFI neurons, and constant excitatory background input. The latter is not considered here, as it is identical for all recurrent neurons and does not convey any visual information. For each recurrent neuron, three tuning curves are extracted: For the mean $\mathrm{I}_{\mathrm{F0}}^{\mathrm{FF}}$ and the amplitude $\mathrm{I}_{\mathrm{F1}}^{\mathrm{FF}}$ of the feedforward input current, and for the mean output firing rate $\nu^{\mathrm{V1}}$. All three types of tuning curves are plotted in Fig 7, for a random sample of recurrent neurons. These curves essentially confirm the outcome of our single-neuron analysis. The mean input current $\mathrm{I}_{\mathrm{F0}}^{\mathrm{FF}}$ is essentially untuned, while the amplitude of $\mathrm{I}_{\mathrm{F1}}^{\mathrm{FF}}$ significantly varies with the orientation of the stimulus (Fig 7, top). The orientation bias in the input is then transformed into responses of recurrent neurons that exhibit a

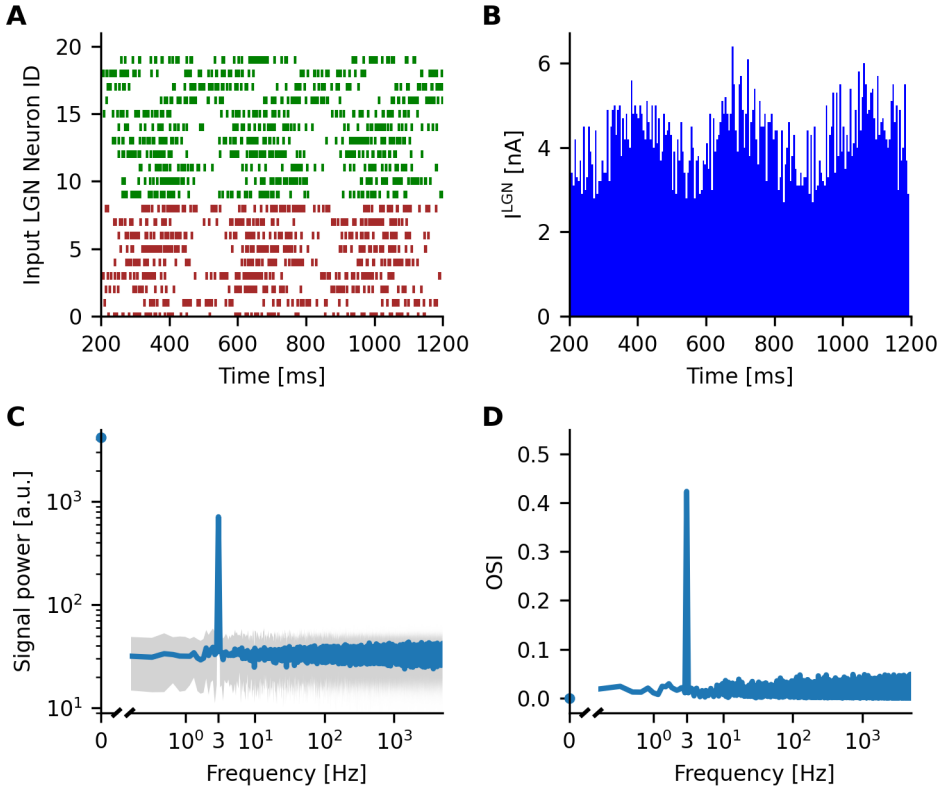


**Fig 6. Compound thalamic inputs to a single V1 neuron. A** Shown are the spike trains of 20 out of 100 afferent dLGN neurons that converge to a specific V1 neuron. Their locations are depicted in Fig 3A. The orientation of the drifting grating stimulus is 60°, its temporal frequency amounts to 3 Hz. **B** Compound thalamic input of all 100 afferents to a single neuron. The current is calculated from the number of spikes arriving in each time bin of the simulation (bin width 5 ms). **C** Power spectral density of the compound input signal computed by Fast Fourier Transform (FFT). The solid blue line represents the mean signal power over 50 trials, each of duration 6 s. The grey shaded area indicates the mean ± standard deviation across trials. **D** Orientation selectivity index (OSI) of the mean signal power, extracted separately for each frequency channel. Significant orientation tuning emerges only for the temporal frequency of the grating at 3 Hz.

pronounced orientation selectivity (Fig 7, bottom).

Next, we jointly quantify the orientation preference of cortical neurons and their corresponding thalamic inputs. The coefficients $\mathrm{PO}_{\mathrm{F0}}^{\mathrm{V1}}$ and $\mathrm{OSI}_{\mathrm{F0}}^{\mathrm{V1}}$ account for the PO and the OSI of the firing rate responses of recurrent V1 neurons, respectively. Since the orientation bias of the compound thalamic input shows up in F1, but not in the F0 component, its tuning is characterized by $\mathrm{PO}_{\mathrm{F1}}^{\mathrm{dLGN}}$ and $\mathrm{OSI}_{\mathrm{F1}}^{\mathrm{dLGN}}$, respectively. Our simulations demonstrate very clearly that orientation selectivity in V1 indeed emerges from random thalamo-cortical projections to a randomly connected network (Fig 8B).

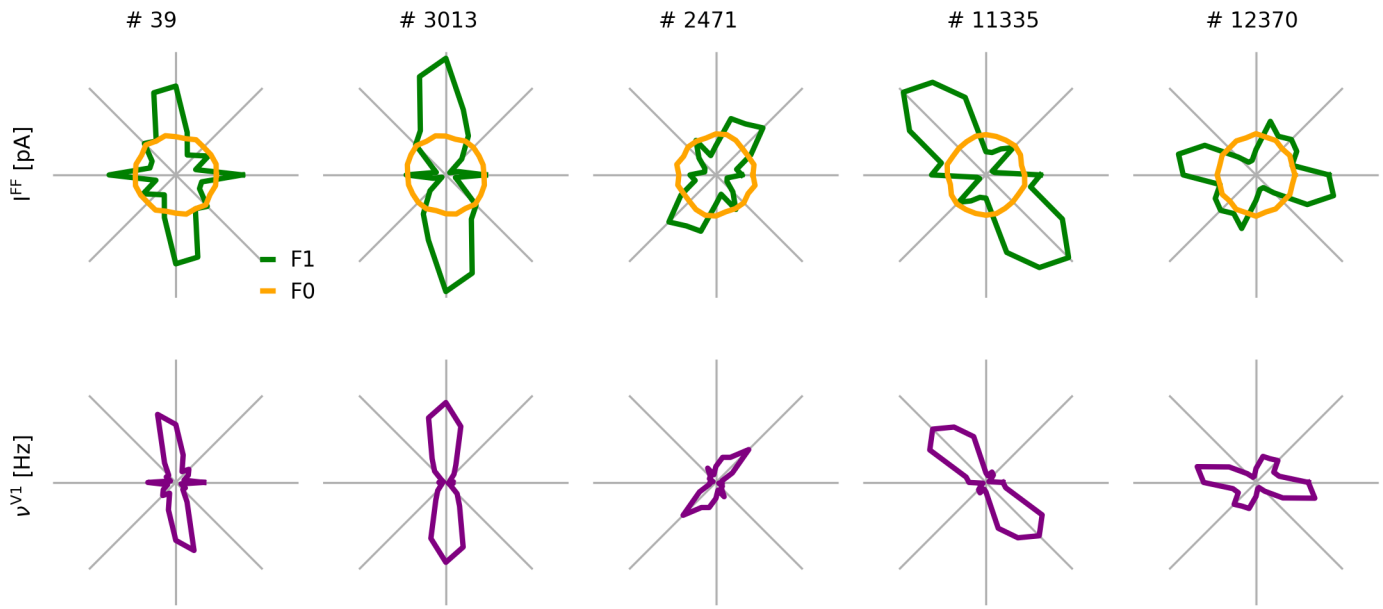


**Fig 7. Input and output tuning curves of V1 neurons.** Examples of matching input (top) and output (bottom) orientation tuning curves in polar representation (360°). The radial axis indicates the F0 (orange) and the F1 (green) component of the input current, as well as the mean output firing rate (purple) for five different neurons, respectively.

Moreover, the output PO and OSI of individual recurrent neurons are strongly correlated to the PO and OSI of their respective thalamic inputs, fully consistent with previous experimental observations [18, 34]. A residual discrepancy between input and output is due to lateral inputs from the recurrent network, as we will demonstrate later.

### Receptive fields in thalamus and cortex

Having shown OS emerging from randomly sampled thalamic inputs, we next investigated the static receptive fields (RF) at all stages of the visual pathway represented in our model and compared them to experimental observations. For stimulation, we used locally sparse noise (Fig S1) and flashed them at a frame rate of 30 Hz. The RFs were then estimated by reverse correlation of the stimulation movie with spiking responses. We mapped the RFs of individual dLGN neurons and cortical recurrent neurons along with their compound input from the thalamus (Fig 9). Individual thalamic neurons had clear-cut center-surround receptive fields, reflecting the design of our model. The RFs of recurrent cortical neurons, in contrast, exhibited patchy excitatory and inhibitory subfields, very similar to what was observed in rodent experiments [12]. Recurrent cortical neurons and their respective thalamic input had in

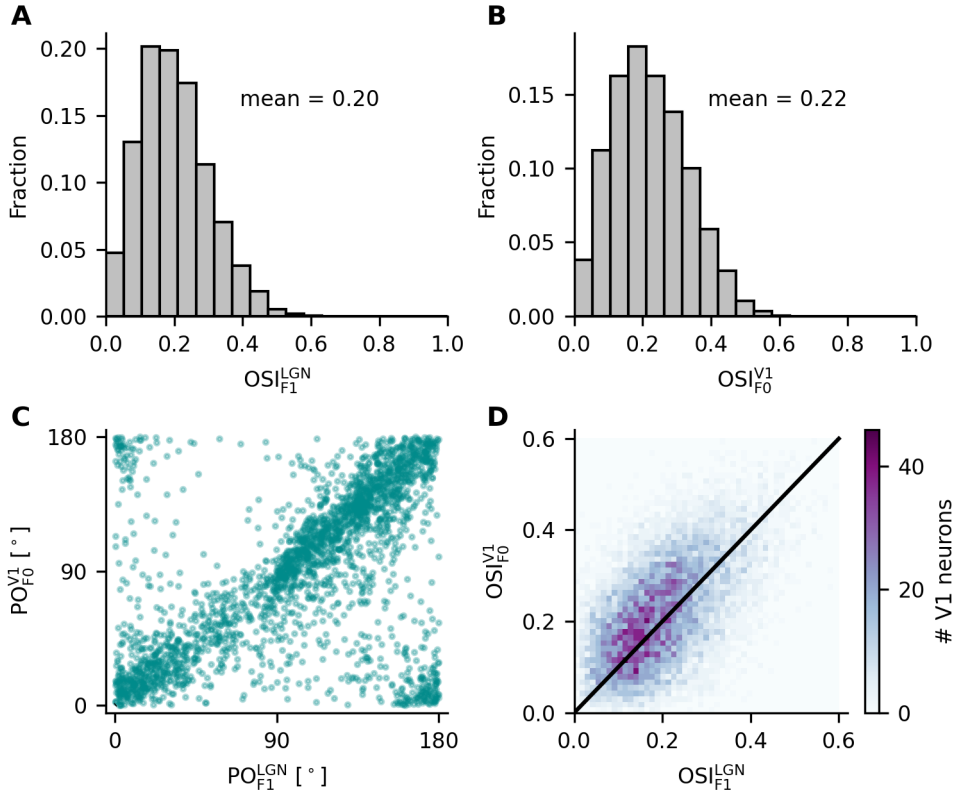


**Fig 8. Orientation selectivity of the V1 population.** Distribution of the OSI for all recurrent excitatory and inhibitory neurons in V1 (**B**) and their respective thalamic compound inputs (**A**). Unlike the output OSI, which is extracted from the orientation tuning of mean firing rates (F0), the input OSI is calculated from the oscillation amplitudes (F1) as the mean input is untuned. The scatter plots for input vs. output PO (**C**) and OSI (**D**) of all neurons show that, on average, the output OSI is slightly larger than the input OSI.

fact highly similar RFs. This confirms that the cortical output is mainly determined by the compound feedforward thalamic input. Note that the samples shown were obtained by spike-triggered averaging over 20 000 frames, but no additional smoothing or fitting was applied.

## Nonlinear transfer of the network

As demonstrated by numerical simulations of spiking networks, orientation selectivity in V1 can emerge from random samples of the visual field at the interface between thalamus and cortex. Cortical neurons amplify the weak orientation bias conveyed by their compound thalamic input. A possible mechanism based on nonlinear signal transfer was explained above, but it was left to be verified that the same mechanism

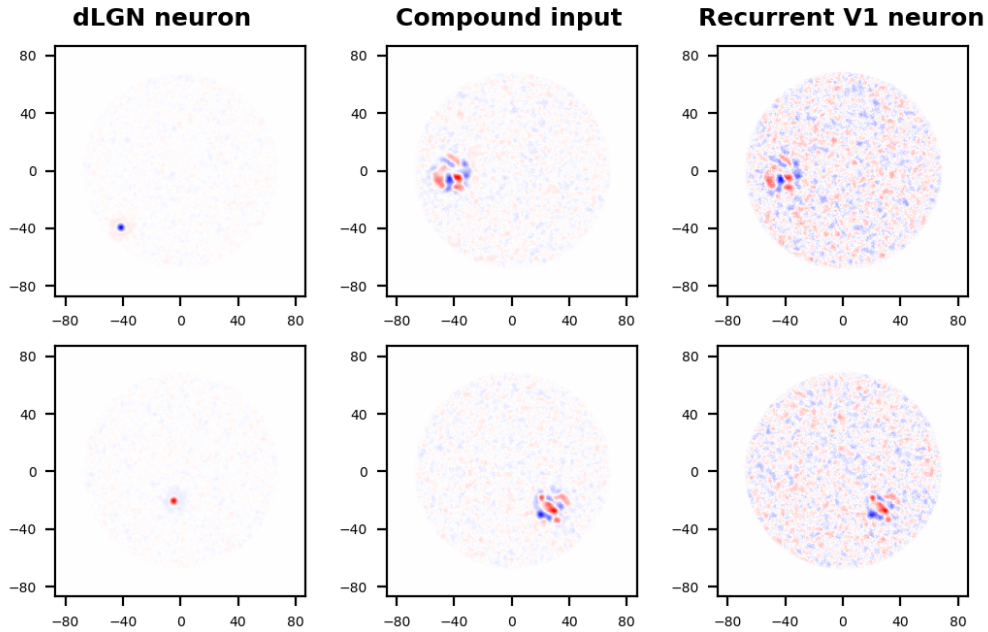


**Fig 9. Receptive fields of dLGN neurons, compound thalamic input, and recurrent V1 neurons.** The receptive fields are extracted by spike-triggered averaging, but no smoothing was applied (see text for details). Shown are two samples of receptive fields for single dLGN neurons (left), compound thalamic inputs (middle) and the corresponding recurrent cortical neurons (right). Blue and red colors show ON and OFF subfields, respectively.

could also cause OS emergence in networks. To this end, we replaced spiking neurons (LIF) by an effective dynamic firing rate model (DRM). Each neuron $i$ in this rate model is characterized by an explicit input-output transfer function $F_i$ (Eq 10), see Materials and methods for more details. As before, we used sinusoidal moving gratings with different orientations as stimuli. Each orientation was presented for a full temporal oscillation period at around 33 ms, arranged in 60 discrete steps. Assuming stationary responses for each step, the output firing rate was computed as a function of the respective input current. This way, we obtained the full time-locked response of input and output (Fig 10A,C). As before, we extracted the transfer function from these data by relating input and output in every moment (Fig 10B). The resulting transfer curve has a characteristic form: With increasing input, the output firing rate of neurons first rises in a convex way and then enters a linear regime. The form of this curve indeed supports OS emergence, provided the operating point can be stabilized by the network.

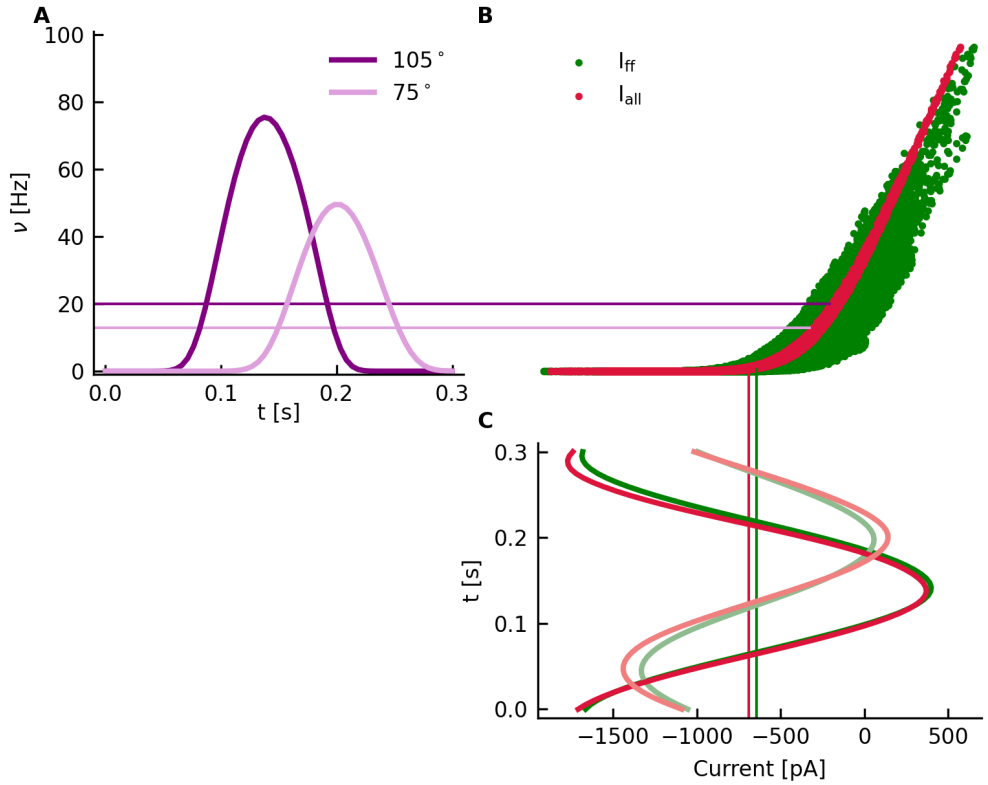


**Fig 10. Nonlinear transfer of the network. A** Time-dependent firing rate of a sample neuron in the recurrent V1 network. The orientation of the stimulus was 75° (lighter colors) and 105° (darker colors). Thin lines represent the temporal mean of the signals with matching colors. **B** The input-output transfer curve of a V1 neuron in the recurrent network. The output firing rate is plotted against the feedforward (green) and total (red) input currents, respectively, as shown in **C**.

### Effect of the recurrent input

Having identified the nonlinear input-output transfer curve of neurons in the network, we went on to characterize the contribution of feedforward and recurrent inputs, respectively, to the emergence of orientation selectivity. To this end, feedforward input current $I_{ff}$ and the total input current $I_{all}$ were calculated separately and plotted against the output firing rates of single neurons. Not surprisingly, feedforward inputs essentially follow the shape of the transfer curve, albeit with some jitter (Fig 10B green). When the recurrent input is also taken into consideration, the input-output transfer curve narrows (Fig 10B red). This demonstrates that the output firing rate is mainly determined by feedforward input and only modified slightly by recurrent input. This explains the strong correlation between preferred orientations of input and output, as

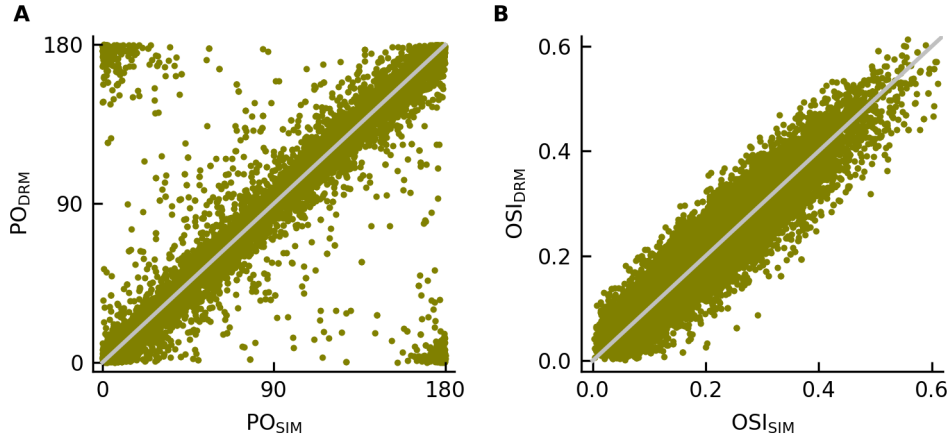


**Fig 11. Performance of the DRM compared to numerical simulations.** The behavior of individual LIF neurons in network simulations is compared to predictions from the dynamic rate model (DRM), see text for details. Shown are scatter plots of PO (**A**) and OSI (**B**) for all recurrent V1 neurons. The gray diagonal line indicates a perfect match.

well as the residual discrepancies between them, observed in simulations (see Fig 8).

### Comparison of spiking neurons and firing rate neurons

In the previous section, we have seen consistent behavior of simulated LIF neurons and the DRM, at different temporal frequencies (Fig 4D). For a moving sinusoidal grating with temporal frequency $f = 3\,\mathrm{Hz}$, the DRM is able to track the dynamics of the input signal. Therefore, it can be considered as a valid approximation of the spiking neuron. A specific comparison of both models at this frequency also yields good consistency with regard to the preferred orientation (PO) and orientation selectivity (OSI) of single neurons (Fig 11), respectively. Residual discrepancies between the two models are explained by fluctuations in the activity of spiking neurons.

## Parameter dependence of orientation selectivity

In the previous paragraph, we have explained a general mechanism how orientation selective responses of recurrent V1 neurons can emerge from random thalamocortical connectivity. Employing a nonlinear transfer function, the F1 tuning in the input is transformed into a F0 tuning curve at the output. As a result, the input F1 component is an essential determinant of the output OS in recurrent V1 neurons. As outlined in

Eq 18, the F1 component of the input depends explicitly on the number of dLGN neurons that converge on a recurrent V1 neuron $K_{\mathrm{V1}}^{\mathrm{dLGN}}$. In addition, it depends on the spatial frequency of the moving grating $\lambda$. In this section, we investigate the detailed dependence of the output OS on these two parameters.

### Thalamo-cortical convergence number

To elucidate the role of the number of thalamo-cortical projections $K_{\mathrm{V1}}^{\mathrm{dLGN}}$ for orientation selectivity of cortical neurons, we determined its impact on the output OSI of recurrent V1 neurons. Throughout all simulations, the size of thalamic receptive fields and the mean current $\mathrm{I}_{\mathrm{F0}}^{\mathrm{dLGN}}$ corresponding to compound thalamic input to V1 neurons were kept fixed. Mean and standard deviation of the OSI across all neurons are depicted for different values of the thalamo-cortical convergence (Fig 12). We found that strong and reliable tuning is obtained for a very broad range of values for $K_{\mathrm{V1}}^{\mathrm{dLGN}}$ between 2 and 1 000 (Fig 12B). Anatomical counts, in fact, yielded numbers in the range between 80 and 200, depending on the animal species [35–37]. If not stated otherwise, the convergence number in our model was set to 100, with an identical number of ON and OFF cells.

We also investigated the dependence of the F1 component of compound thalamic input on the number of convergent inputs, as it represents the most important determinant of the output orientation preference. For increasing convergence numbers, the oscillation amplitude of the compound thalamic input current $\mathrm{I}_{\mathrm{F1}}^{\mathrm{dLGN}}$ decreases (Fig 12C), while the average OSI of the input amplitude remains at a fixed level (Fig 12A). As a result of nonlinear signal transfer, the output OSI depends on the convergence number in a complex manner (Fig 12B). When the convergence number is low, the oscillation amplitude is large, resulting in high output firing rate. In this case, the operating point is almost shifted outside the nonlinear range, and the output OSI becomes smaller. When the convergence number gets larger, the input OSI remains unchanged, but the oscillation amplitude decreases. Therefore, the output OSI declines as the oscillation is amplified less. Overall, the orientation selectivity of the output does not only depend on the oscillation amplitude of the thalamic input $\mathrm{I}_{\mathrm{F1}}^{\mathrm{dLGN}}$, but also its orientation selectivity $\mathrm{OSI}_{\mathrm{F1}}^{\mathrm{dLGN}}$.

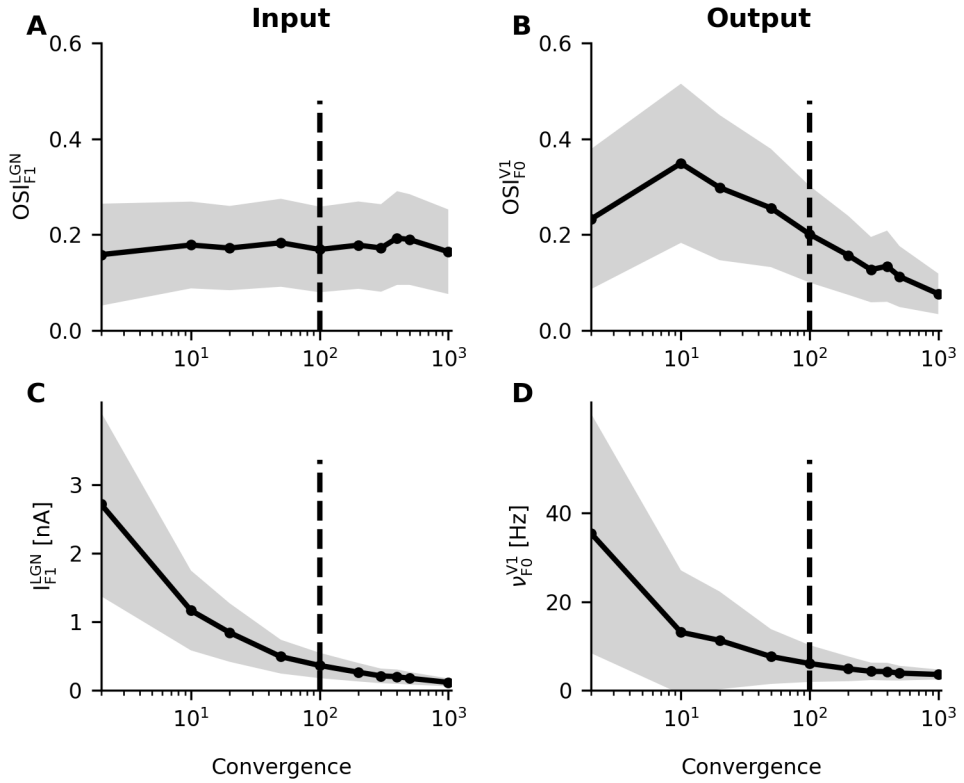


**Fig 12. Thalamo-cortical convergence and orientation selectivity.** Four quantities are plotted against the number of thalamic afferents converging on a single cortical neuron: **A** The OSI of oscillation amplitudes of compound thalamic input, **B** the OSI of firing rate output in recurrent neurons, **C** the amplitude of compound thalamic current oscillations, and **D** the mean firing rate of recurrent neurons. Solid lines and gray shaded areas represent mean ± standard deviation. Depending on the animal species, convergence numbers between 80 and 200 have been reported. A convergence number of 100 was chosen in most of our simulations (dashed line).

### Spatial frequency affects orientation tuning

We next investigated how the orientation preference of recurrent V1 neurons depends on the spatial frequency of the stimulus. Sinusoidal moving gratings at different spatial frequencies ranging from 0.001 to 0.4 cycles per degree (cpd) were used as visual stimuli. Orientation preference (PO and OSI) was extracted from the single-neuron tuning curves at each spatial frequency. For the network layout considered in our model, strongest tuning was observed between 0.06 and 0.08 cpd, and the tuning became rather weak for very small (below 0.003 cpd) and for very large (above 0.3 cpd) spatial frequencies (Fig 13A). This shows that the strength of orientation tuning (OSI) of the output is affected by the spatial frequency of the stimulus, and the strongest tuning was

obtained for a spatial frequency at about 0.08 cpd. In addition, we observed that the preferred orientation (PO) of single neurons was different for different spatial frequencies. To quantify the changes in PO, we first determined the PO for different spatial frequencies, for all neurons in the network. Separately for each spatial frequency, we then calculated the circular correlation (see Materials and methods) of these angular variables with the PO obtained for the same neuron at the reference spatial frequency of 0.08 cpd. The correlation is higher for similar frequencies and lower for very distant frequencies (Fig 13B). The correlation coefficient is around 0.35 for 0.07 cpd (Fig 13D), while it is close to 0 for 0.01 cpd (Fig 13E). Similar observations were also made in experiments in rodents and higher mammals. The spatial frequency has generally a strong impact on the OSI, and different spatial frequencies lead to a different PO in single neurons [11, 21]. Note that, as a matter of principle, a model of primary visual processing that specifies the receptive fields of cortical neurons in terms of *a priori* excitatory and inhibitory subfields cannot explain such dependencies.

## Contrast-invariant orientation tuning

The perceived orientation of a stimulus should, ideally, not depend on the stimulus contrast. Contrast-invariant tuning curves are indeed widely observed in the visual cortex of cats as well as mice [2, 3, 38]. Here, we report that contrast-invariance of orientation tuning is also a property of neuronal responses in our model. Sinusoidal drifting gratings with contrasts varying between 0 and 1 (see Materials and methods) were presented for 12 different orientations, as described before. Note that the mean luminosity of the grating remained unchanged for the different contrasts considered here. As a consequence, the mean firing rates of dLGN neurons were unchanged as well, while stimulus contrast was reflected by the amplitude of temporal oscillations. For zero contrast, the sinusoidal grating is just a uniform gray with mean luminosity everywhere. Clearly, no stimulus orientation can be observed under this condition. Although the response amplitudes at the preferred orientation are higher for stronger contrasts, the general shape of the tuning curves does not depend on contrast (examples see Figure 14C,D).

To investigate the impact of stimulus contrast on orientation preference, the PO and

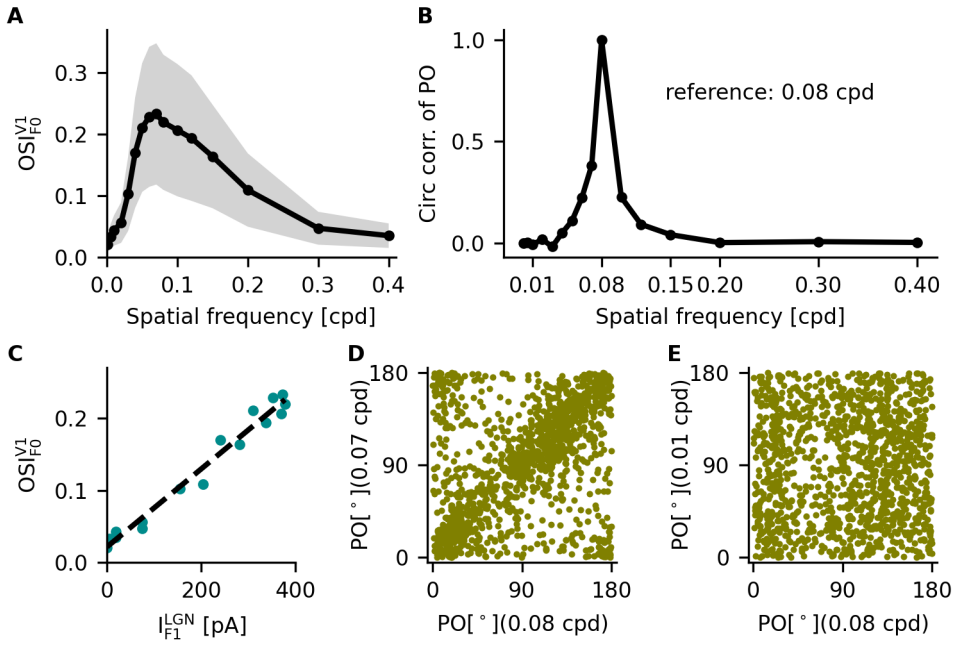


**Fig 13. Influence of spatial frequency on orientation selectivity. A** The OSI depends on the spatial frequency of the drifting grating used for stimulation in the model. The solid curve and the gray shaded area represent mean ± standard deviation. **B** The PO of individual neurons in the same network changes with the spatial frequency of the grating. The PO at 0.08 cpd is very different from the PO for deviating spatial frequencies, as indicated by the circular correlation coefficient. **C** The oscillation amplitude of compound input current is the most important determinant for the OSI of the output firing rate in recurrent neurons. **D,E** A similar picture emerges by directly comparing the PO of all recurrent neurons at similar spatial frequencies (0.07 vs. 0.08 cpd) and at strongly deviating spatial frequencies (0.01 vs. 0.08 cpd).

the OSI of single neurons were extracted. We found that the OSI was generally proportional to contrast (Fig 14A). This reflects the fact that the tuning strength is related to the signal-to-noise ratio, which is here determined by the amplitude of temporal oscillations and the offset. We also quantified the stability of tuning by calculating the absolute PO difference for single neurons at reduced contrasts compared to the maximum contrast 1. Fig 14B demonstrates that the PO extracted from simulated spike trains is rather stable. For very low contrasts, however, low signal-to-noise ratios do not support reliable estimates of the PO. Our analysis supports the notion that orientation tuning curves are contrast-invariant, similarly as reported from experiments.

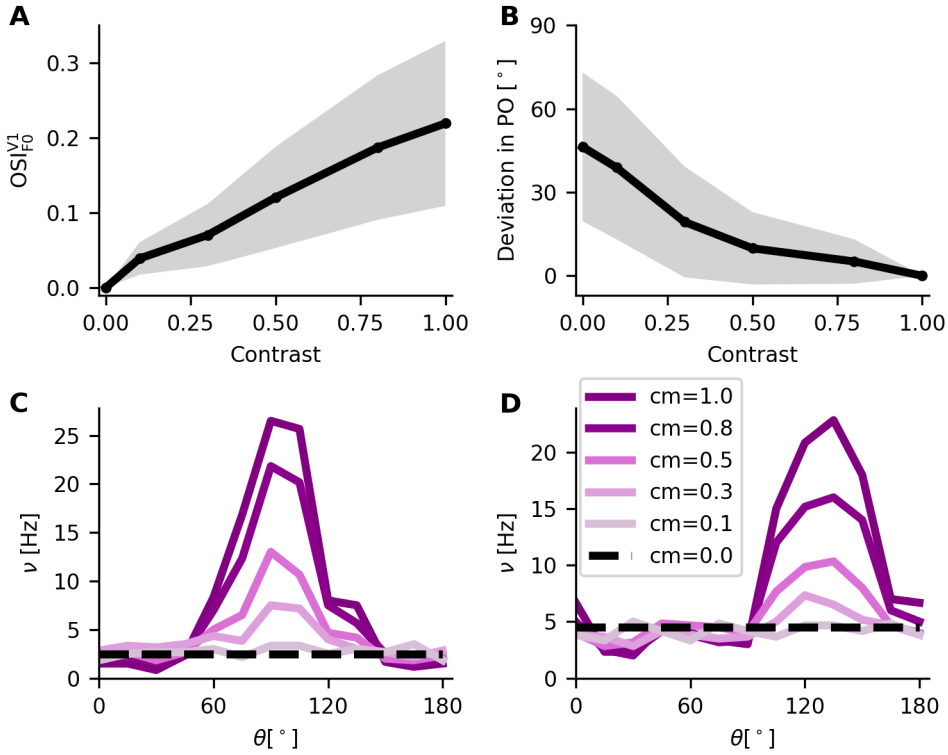


**Fig 14. Contrast-invariance of tuning curves. A** Shown is the OSI of V1 neurons for different values of the stimulus contrast (mean ± standard deviation). **B** Deviation of the PO in degrees for a stimulus of reduced contrast (indicated on the x-axis) as compared to maximal contrast (1). **C,D** Sample tuning curves for one excitatory (left) and one inhibitory (right) neuron, at different contrasts of the stimulus. Lighter colors represent lower contrasts. Dashed lines indicate the neuronal responses at 0 contrast.

# Discussion

Deviating from Hubel and Wiesel's [1] original suggestion based on experiments in cat visual cortex, we explored the possibility that orientation selectivity in rodent visual cortex is mediated by unstructured random projections from thalamus to cortex. Our analysis proceeded in three stages: First, we described how sparse random sampling of the receptive field can generate a compound feedforward signal at the interface between thalamus and cortex with a significant orientation bias. Second, we analysed how nonlinear signal transduction in a generic neuron model can transform the input bias into orientation selective neuronal responses. Third, we devised a thalamocortical network model to identify the minimal circuit that can reliably support contrast-invariant tuning curves of V1 neurons.

Based on our new model, we analyzed the neuronal circuit computations underlying

OS emergence. Our simulation results were widely compatible with experimental measurements in rodents. We first verified in our model that the mean thalamic input is the same for all orientations of a drifting grating, while the temporal oscillation amplitude of the compound signal has an orientation bias, exactly as reported in experiments in rodents [18]. We then demonstrated that this orientation bias is transformed into orientation selective firing rates of V1 neurons, mediated by a generic nonlinear transfer inherent to all neurons. Feedforward inhibition and recurrent inhibition in the cortex must be properly arranged to compensate any untuned offset of thalamic input and to stabilize the operating point of the nonlinear transfer. The numerical simulation of our model revealed that the orientation selectivity of the output depends on the number of dLGN afferents, matching the numbers known from different animal species [35]. The emergent tuning curves also depend on the spatial frequency of the grating used for stimulation, similar to what has been found in experiments [2, 11]. As the described mechanisms are very general, they might account for the emergence of feature selectivity in other sensory modalities as well, provided the information is conveyed in the amplitude of oscillations.

## Orientation tuning of dLGN neurons

In our model, by design, dLGN neurons respond equally to all stimulus orientations. Orientation selective responses of V1 neurons emerge, for the first time, at the interface between thalamus and cortex. In contrast to single dLGN neurons, the oscillation amplitude of compound thalamic inputs has a significant orientation bias. This amplitude bias (F1) is transformed into a bias of firing rates (F0). Contrast-invariant tuning curves result with the help of recurrent inhibition in the V1 network.

Since orientation selectivity was first described in cat visual cortex by Hubel and Wiesel, it has long been thought that individual dLGN neurons convey only untuned inputs to the visual cortex. However, recent experimental studies in mice revealed that some dLGN relay cells are somewhat orientation selective [10, 39]. These tuned dLGN cells indeed project to layer 4, the main input layer of V1 [40]. In our network model, the mean and dispersion of orientation selectivity across cortical neurons is a bit smaller than reported in experiments [3, 12]. Accounting for individual thalamic inputs with

orientation preference will increase the tuning of the input amplitude and, therefore, also yields slightly stronger orientation selectivity in V1 neurons. This brings our model even closer to experimental findings.

## Contribution of the input amplitude

In the model developed here, the orientation bias in the amplitude of input oscillations is transformed into orientation tuning of output firing rate, exploiting generic nonlinear properties of neurons. The mean input, which is the same for all stimulus orientations, sets the operating point. Unfavorable combinations of parameters, however, may compromise the nonlinear transduction and attenuate the output tuning. Our analysis revealed that orientation selectivity of the output is mainly determined by the amplitude of input oscillations (Fig 8D, Fig 12, Fig 13C). On the one hand, small oscillation amplitudes render the nonlinear transduction mechanism ineffective. On the other hand, large input amplitudes can lead to low output selectivity, if the modulation of the input amplitude is small. The magnitude $\mathrm{I}_{\mathrm{F1}}^{\mathrm{dLGN}}$ as well as the modulation $\mathrm{OSI}_{\mathrm{F1}}^{\mathrm{dLGN}}$ of input amplitude work together to determine the output selectivity of V1 neurons.

## Role of feedforward inhibition

To achieve optimal orientation selectivity of firing rates, it is important to stabilize the operating point in the nonlinear regime of the neuronal transfer function. In the thalamocortical network model considered here, the untuned component of the thalamic input is compensated by feedforward inhibition, and a stable F1-to-F0 transformation is enabled. Feedforward inhibition is generally associated with parvalbumin (PV) expressing GABAergic interneurons. In experiments, it has indeed been shown that PV neurons provide untuned feedforward inhibition to excitatory neurons in V1 [41]. In addition, layer 4 PV interneurons are directly innervated by thalamocortical axons in layer 4 [42, 43]. Fast spiking basket cells, a subtype of PV interneurons, were explicitly shown to mediate the feedforward inhibition of thalamocortical inputs. These findings are consistent with the role assigned to feedforward inhibition in our network model: These interneurons are mainly driven by thalamic input, they typically fire at high rates, and their output provides essentially untuned inhibitory input to recurrent V1 neurons.

Besides feedforward inhibition in our network, there are other known pathways which might contribute to a stabilization of the baseline of thalamic input. For instance, the thalamic reticular nucleus (TRN) is comprised exclusivley of GABAergic interneurons and can make an indirect contribution being involved in a corticothalamic pathway. In this feedback loop, TRN cells receive input from both thalamus and cortical layer 6 and then exclusively project to thalamic nuclei. This extended recurrent circuit might control the excitation of thalamocortical relay cells and this way modulate thalamic signaling [44–47].

## Choice of the neuron model

The emergence of orientation selectivity in our model depends on an essential way on the generic nonlinear transmission properties of neurons. In our simulations, all neurons are conceived as current-based leaky integrate-and-fire (LIF) point neurons. The question arises whether cortical nerve cells in particular are well represented by this simplistic neuron model. Despite the lack of structured dendrites and detailed intrinsic conductances, however, the LIF neuron model is able to capture fundamental processes performed by biological nerve cells, namely synaptic input integration and spike-based signaling. This generic model is, in fact, the most widely used model to study the dynamic behavior of large recurrent networks [19] and has been found useful in studying information processing in neural networks [48]. Therefore, the LIF model is a natural and adequate choice to also study the generic mechanisms underlying thalamocortical signal processing.

## Consistency with experiments

The results of our model-based analysis are widely consistent with observations reported in mouse experiments. While the F0 component of thalamic input in our model is essentially untuned to stimulus orientation, the F1 component has a significant orientation bias. This initial bias is then transformed into strong and contrast-invariant orientation tuning in recurrent V1 neurons. Exactly the same phenomenon has been observed in recordings from layer 4 neurons of mouse visual cortex: The F1 modulation of thalamic excitatory input is tuned to the orientation of the stimulus, while the total

excitatory postsynaptic charge, which is equivalent to the F0 component, is the same for all orientations [18]. A key role of visual cortex in transforming and amplifying the tuned thalamic input was also demonstrated in these experiments. In our model, the orientation preference of V1 neuronal responses is strongly correlated with the preferred orientation of their thalamic inputs. The output has a slightly stronger orientation selectivity (measured by the OSI) than the input (Fig 8 C,D). The orientation selectivity of recurrent V1 neurons in the model, however, is somewhat smaller than reported in experiments [21, 39]. On the one hand, tuned input from the thalamus, which is not considered in our model, would also increase cortical orientation selectivity. On the other hand, thalamocortical projections in animals are not as random as assumed in our model. Nonrandom spatial sampling of TC projections will typically also enhance the orientation selectivity of cortical neurons. The spatial frequency of the visual stimulus, as found in experiments [11] has a strong impact on the preferred orientation as well as the strength of the orientation selectivity.

## Comparison with alternative models

Most previous theoretical accounts of orientation selectivity referred to recordings from cats and primates [20, 49, 50]. These models assume that the projections from retinal ganglion cells to cortical neurons pass through dLGN without modification. The emergence of orientation selectivity from random inputs is due to distance-dependent connectivity between them, and orientation columns naturally emerge in this scenario. Orientation preferences of V1 neurons in rodents, however, do not seem to be neatly organized in smooth maps [8], and the salt-and-pepper distribution of different preferences does not suggest spatial models to be applicable.

It has been previously suggested [21] that orientation selectivity could emerge from random connectivity, without the dedicated alignment of sensors [1], and in absence of orientation maps [8]. The explanation offered by Pattadkal and colleagues was that orientation-selective responses of cortical neurons could be the result of randomly emerging ON and OFF subfields of thalamic inputs. The random orientation bias in the thalamic input would then be maintained by the excitatory-inhibitory cortical network. Under these conditions, it was found that the OSI was robust with regard to the

number of thalamo-cortical projections and spatial frequency of the stimulus (apart from very low frequencies), while the PO itself depended strongly on spatial frequency.

Adopting the same general idea in our new work, we have come up with a different explanation of the phenomenon by emphasizing other aspects of the computations performed by the thalamo-cortical circuit. In our model, similar to previous work, we also assumed projections from thalamus to cortex with no particular *a priori* structure. Each individual cortical neuron thus performs a random sampling of the visual field. If stimulated with a moving grating, the resulting compound input had a temporal modulation following the grating with a phase resulting from the interference of many oscillatory inputs of different phases. The amplitude of these resulting oscillations was tuned to orientation, in full agreement with experimental findings [18]. Our analysis revealed that the F1-to-F0 transformation is naturally mediated by the nonlinear input-output transfer performed by individual neurons (see Fig 10G). Combining these two effects, our theory shows explicitly how the tuning of cortical neurons depends on the thalamo-cortical convergence number and on the spatial frequency of the stimulus (see Fig 12 and Fig 13). Compared to previous models, therefore, our model did not only exhibit reliable tuning in numerical simulations, but it also explained the detailed neuronal mechanisms underlying the emergence of contrast-invariant tuning curves in V1 neurons.

## Conclusion

Our modeling study revealed that random connectivity can, in principle, account for the emergence of orientation selectivity, and we identified a neuronal mechanism that might underlie it. For this nonlinear mechanism to work properly, it is crucial to stabilize the operating point of feedforward thalamocortical projections. Under these conditions, the thalamic input (F1) tuning is transformed into cortical output (F0) tuning. Our results suggest that no specific spatial configuration of the afferent receptive fields is required to induce orientation selectivity. Moreover, we devised a dynamic firing rate model which can account for slow oscillatory input without solving the time-dependent Fokker-Planck equation. We could confirm the experimental finding that the spatial frequency of the grating has a significant impact on the emerging orientation selectivity.

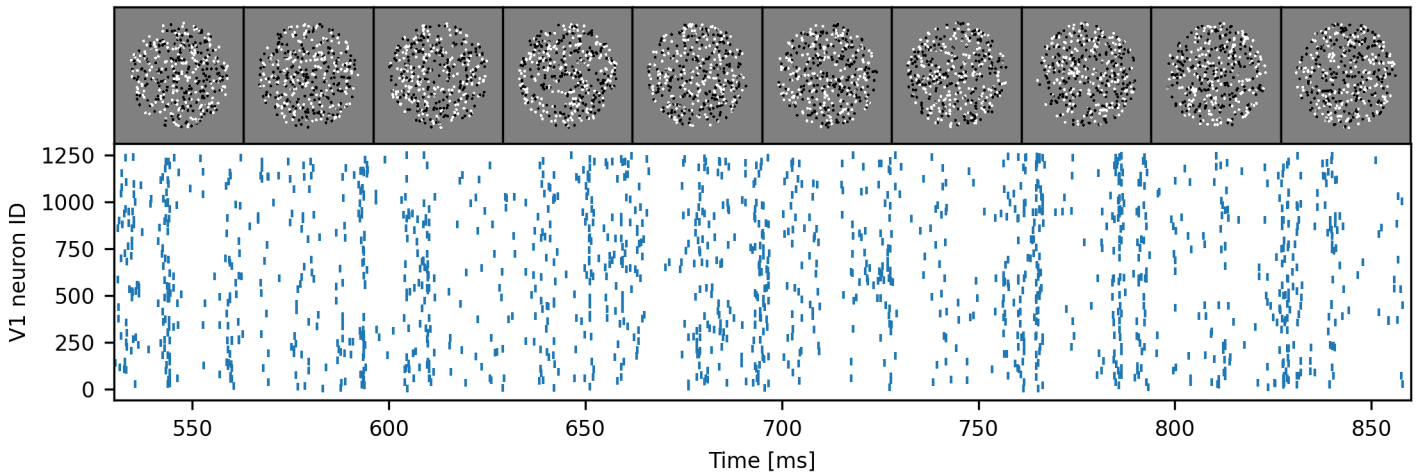


**Fig S1. Receptive field measurement by reverse correlation.** The top row shows sample frames of a sparse spot stimulus. Each frame is presented for 33 ms. The bottom raster plots show the spikes of V1 neurons (10% of the whole population) that were elicited by sparse spot stimulation.

In addition, our model might also provide new insight into computations in other sensory systems that rely on the processing of oscillatory signals.

## Supporting information

## Acknowledgments

This work was partially funded by the joint training program SMARTSTART, launched by the Bernstein Network Computational Neuroscience and the Volkswagen Foundation. Additional support was obtained from the European Union's Seventh Framework Programme (FP7/2007-2013) under Grant Agreement 600925 (NeuroSeeker) and from the DFG (grant EXC 1086). The HPC facilities used for this work are funded by the state of Baden-Württemberg through bwHPC and DFG grant INST 39/963-1 FUGG. In addition, our work was promoted by the German Academic Exchange Service (DAAD) and the Carl Zeiss Stiftung. The funders had no role in study design, data collection and analysis, decision to publish, or preparation of the manuscript.

We thank Uwe Grauer from the Bernstein Center Freiburg as well as Bernd Wiebelt and Michael Janczyk from the Freiburg University Computing Center for their assistance with HPC applications and the developers of the neural simulation tool NEST.

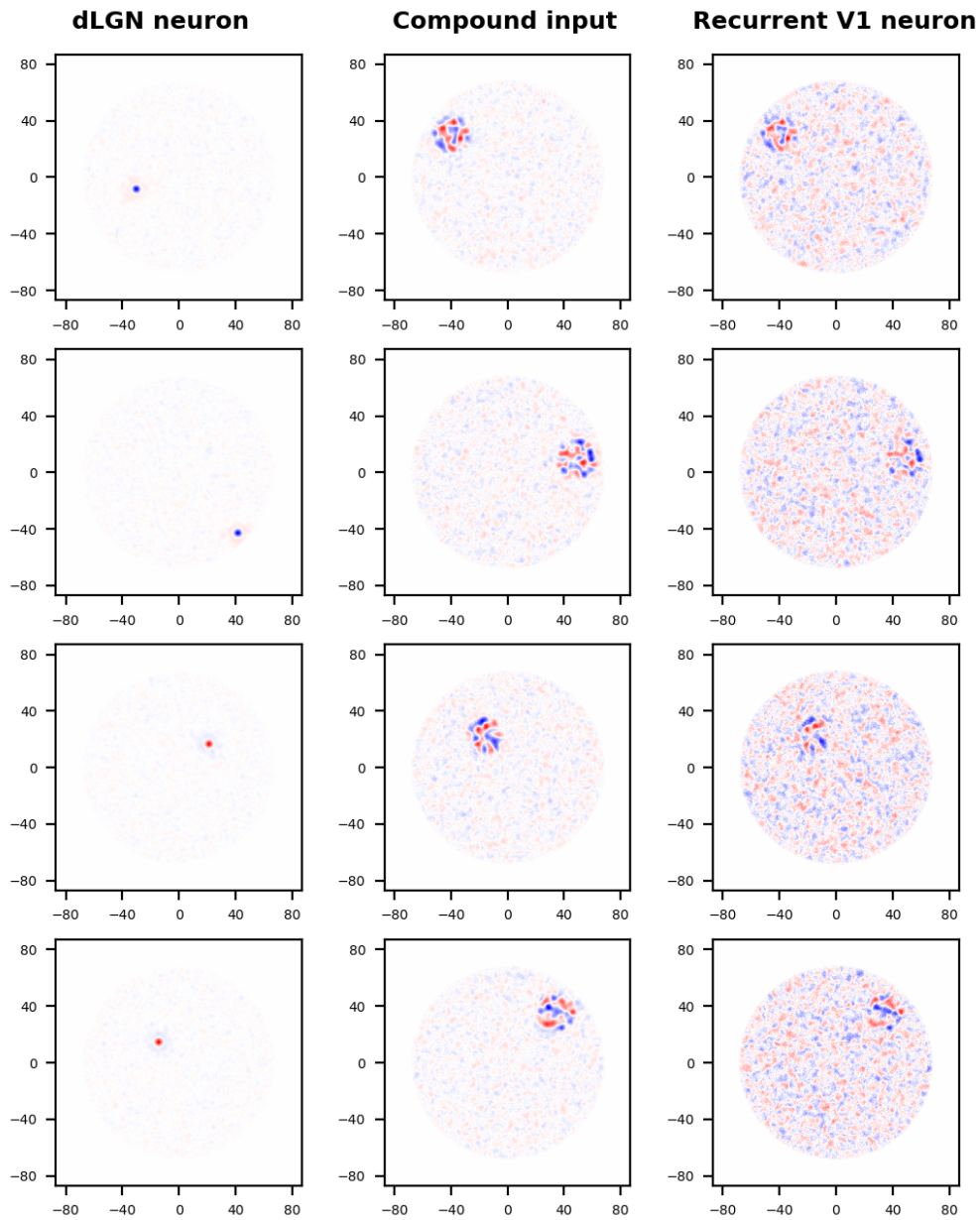


**Fig S2. Examples of receptive fields.** Shown are four more examples of RFs related to Fig 9. Blue and red colors show ON and OFF subfields.

We also thank Philippe Coulon and Nebojša Gašparović for their valuable advises.

## References


1. Hubel DH, Wiesel TN. Receptive fields, binocular interaction and functional architecture in the cat's visual cortex. The Journal of physiology. 1962;160(1):106–154.

2. Ferster D, Miller KD. Neural mechanisms of orientation selectivity in the visual cortex. Annual review of neuroscience. 2000;23(1):441–471.

3. Niell CM, Stryker MP. Highly selective receptive fields in mouse visual cortex. Journal of Neuroscience. 2008;28(30):7520–7536.

4. McLaughlin D, Shapley R, Shelley M, Wielaard DJ. A neuronal network model of macaque primary visual cortex (V1): Orientation selectivity and dynamics in the input layer 4C$\alpha$. Proceedings of the National Academy of Sciences. 2000;97(14):8087–8092.

5. Kremkow J, Jin J, Wang Y, Alonso JM. Principles underlying sensory map topography in primary visual cortex. Nature. 2016;533(7601):52.

6. Hubel DH, Wiesel TN. Ferrier lecture: Functional architecture of macaque monkey visual cortex. Proceedings of the Royal Society of London Series B, Biological Sciences. 1977; p. 1–59.

7. Blasdel GG, Salama G. Voltage-sensitive dyes reveal a modular organization in monkey striate cortex. Nature. 1986;321(6070):579.

8. Ohki K, Chung S, Ch'ng YH, Kara P, Reid RC. Functional imaging with cellular resolution reveals precise micro-architecture in visual cortex. Nature. 2005;433(7026):597.

9. Hofer SB, Ko H, Pichler B, Vogelstein J, Ros H, Zeng H, et al. Differential connectivity and response dynamics of excitatory and inhibitory neurons in visual cortex. Nature neuroscience. 2011;14(8):1045.

10. Tang J, Jimenez SCA, Chakraborty S, Schultz SR. Visual receptive field properties of neurons in the mouse lateral geniculate nucleus. PloS one. 2016;11(1):e0146017.

11. Ayzenshtat I, Jackson J, Yuste R. Orientation tuning depends on spatial frequency in mouse visual cortex. eNeuro. 2016;3(5).

12. Ko H, Cossell L, Baragli C, Antolik J, Clopath C, Hofer SB, et al. The emergence of functional microcircuits in visual cortex. Nature. 2013;496(7443):96.

13. Priebe NJ. Mechanisms of orientation selectivity in the primary visual cortex. Annual review of vision science. 2016;2:85–107.

14. Hansel D, van Vreeswijk C. The mechanism of orientation selectivity in primary visual cortex without a functional map. Journal of Neuroscience. 2012;32(12):4049–4064.

15. Pehlevan C, Sompolinsky H. Selectivity and sparseness in randomly connected balanced networks. PLoS One. 2014;9(2):e89992.

16. Sadeh S, Cardanobile S, Rotter S. Mean-field analysis of orientation selectivity in inhibition-dominated networks of spiking neurons. SpringerPlus. 2014;3(1):148.

17. Sadeh S, Rotter S. Orientation selectivity in inhibition-dominated networks of spiking neurons: effect of single neuron properties and network dynamics. PLoS computational biology. 2015;11(1):e1004045.

18. Lien AD, Scanziani M. Tuned thalamic excitation is amplified by visual cortical circuits. Nature neuroscience. 2013;16(9):1315.

19. Brunel N. Dynamics of sparsely connected networks of excitatory and inhibitory spiking neurons. Journal of computational neuroscience. 2000;8(3):183–208.

20. Von der Malsburg C. Self-organization of orientation sensitive cells in the striate cortex. Kybernetik. 1973;14(2):85–100.

21. Pattadkal JJ, Mato G, van Vreeswijk C, Priebe NJ, Hansel D. Emergent orientation selectivity from random networks in mouse visual cortex. Cell reports. 2018;24(8):2042–2050.

22. Braitenberg V, Schüz A. Cortical architectonics. In: Cortex: Statistics and geometry of neuronal connectivity. Springer; 1998. p. 135–137.

23. Gil Z, Connors BW, Amitai Y. Efficacy of thalamocortical and intracortical synaptic connections: quanta, innervation, and reliability. Neuron. 1999;23(2):385–397.

24. Richardson RJ, Blundon JA, Bayazitov IT, Zakharenko SS. Connectivity patterns revealed by mapping of active inputs on dendrites of thalamorecipient neurons in the auditory cortex. Journal of Neuroscience. 2009;29(20):6406–6417.

25. Gewaltig MO, Diesmann M. Nest (neural simulation tool). Scholarpedia. 2007;2(4):1430.

26. Fardet T, Vennemo SB, Mitchell J, Mørk H, Graber S, Hahne J, et al.. NEST 2.20.0; 2020. Available from: `https://doi.org/10.5281/zenodo.3605514`.

27. Siegert AJ. On the first passage time probability problem. Physical Review. 1951;81(4):617.

28. Ricciardi LM. The first passage time problem. In: Diffusion Processes and Related Topics in Biology. Springer; 1977. p. 61–72.

29. Amit DJ, Tsodyks M. Quantitative study of attractor neural network retrieving at low spike rates. I. Substrate-spikes, rates and neuronal gain. Network: Computation in neural systems. 1991;2(3):259.

30. Batschelet E, Batschelet E, Batschelet E, Batschelet E. Circular statistics in biology. vol. 111. Academic press London; 1981.

31. Piscopo DM, El-Danaf RN, Huberman AD, Niell CM. Diverse visual features encoded in mouse lateral geniculate nucleus. Journal of Neuroscience. 2013;33(11):4642–4656.

32. Ringach D, Shapley R. Reverse correlation in neurophysiology. Cognitive Science. 2004;28(2):147–166.

33. Waldert S, Pistohl T, Braun C, Ball T, Aertsen A, Mehring C. A review on directional information in neural signals for brain-machine interfaces. Journal of Physiology-Paris. 2009;103(3-5):244–254.

34. Li Yt, Ibrahim LA, Liu Bh, Zhang LI, Tao HW. Linear transformation of thalamocortical input by intracortical excitation. Nature neuroscience. 2013;16(9):1324.

35. Alonso JM, Usrey WM, Reid RC. Rules of connectivity between geniculate cells and simple cells in cat primary visual cortex. Journal of Neuroscience. 2001;21(11):4002–4015.

36. Peters A, Payne BR. Numerical relationships between geniculocortical afferents and pyramidal cell modules in cat primary visual cortex. Cerebral Cortex. 1993;3(1):69–78.

37. Potjans TC, Diesmann M. The cell-type specific cortical microcircuit: relating structure and activity in a full-scale spiking network model. Cerebral cortex. 2012;24(3):785–806.

38. Priebe NJ, Ferster D. Inhibition, spike threshold, and stimulus selectivity in primary visual cortex. Neuron. 2008;57(4):482–497.

39. Scholl B, Tan AY, Corey J, Priebe NJ. Emergence of orientation selectivity in the mammalian visual pathway. Journal of Neuroscience. 2013;33(26):10616–10624.

40. Sun W, Tan Z, Mensh BD, Ji N. Thalamus provides layer 4 of primary visual cortex with orientation-and direction-tuned inputs. Nature neuroscience. 2016;19(2):308.

41. Ma Wp, Liu Bh, Li Yt, Huang ZJ, Zhang LI, Tao HW. Visual representations by cortical somatostatin inhibitory neurons—selective but with weak and delayed responses. Journal of Neuroscience. 2010;30(43):14371–14379.

42. Rudy B, Fishell G, Lee S, Hjerling-Leffler J. Three groups of interneurons account for nearly 100% of neocortical GABAergic neurons. Developmental neurobiology. 2011;71(1):45–61.

43. Ji Xy, Zingg B, Mesik L, Xiao Z, Zhang LI, Tao HW. Thalamocortical innervation pattern in mouse auditory and visual cortex: laminar and cell-type specificity. Cerebral Cortex. 2015;26(6):2612–2625.

44. Sherman SM. Functioning of circuits connecting thalamus and cortex. Comprehensive Physiology. 2011;7(2):713–739.

45. Sherman SM. Thalamus plays a central role in ongoing cortical functioning. Nature neuroscience. 2016;19(4):533.

46. Neyer C, Herr D, Kohmann D, Budde T, Pape HC, Coulon P. mGluR-mediated calcium signalling in the thalamic reticular nucleus. Cell Calcium. 2016;59(6):312–323.

47. Coulon P, Herr D, Kanyshkova T, Meuth P, Budde T, Pape HC. Burst discharges in neurons of the thalamic reticular nucleus are shaped by calcium-induced calcium release. Cell calcium. 2009;46(5-6):333–346.

48. Burkitt AN. A review of the integrate-and-fire neuron model: I. Homogeneous synaptic input. Biological cybernetics. 2006;95(1):1–19.

49. Soodak RE. The retinal ganglion cell mosaic defines orientation columns in striate cortex. Proceedings of the National Academy of Sciences. 1987;84(11):3936–3940.

50. Ringach DL. Haphazard wiring of simple receptive fields and orientation columns in visual cortex. Journal of neurophysiology. 2004;92(1):468–476.

| | | |
|---|---|---|
| **Network connectivity** | | |
| Number of V1 neurons | $N$ | 12 500 |
| Recurrent connection probability | $\epsilon$ | 10% |
| Number of dLGN neurons | $N_{\mathrm{dLGN}}$ | 3 071 |
| Number of FFi neurons | $N_{\mathrm{FFI}}$ | 1 500 |
| Projection number of dLGN→V1 | $K_{\mathrm{V1}}^{\mathrm{dLGN}}$ | 100 |
| Projection number of dLGN→FFi | $K_{\mathrm{FFI}}^{\mathrm{dLGN}}$ | 8 |
| Projection number of FFi→V1 | $K_{\mathrm{V1}}^{\mathrm{FFI}}$ | 320 |
| **Neuron model** | | |
| Membrane time constant | $\tau_{\mathrm{m}}$ | 20 ms |
| Refractory period | $\tau_{\mathrm{ref}}$ | 2 ms |
| Membrane resistance | R | 40 MΩ |
| Membrane capacitance | $C_{\mathrm{m}}$ | 250 pF |
| Resting potential | $V_{\mathrm{r}}$ | 0 mV |
| Threshold voltage of V1 neurons | $V_{\mathrm{th}}$ | 20 mV |
| Threshold voltage of FFi neurons | $V_{\mathrm{th}}^{\mathrm{FFI}}$ | 20 mV |
| **Synaptic model** | | |
| Synaptic delay | $D$ | 1.5 ms |
| Recurrent exc. synaptic efficacy | $J_{\mathrm{E}}$ | 0.2 mV |
| Inhibition dominance ratio | $g$ | 8 |
| Recurrent inh. synaptic efficacy | $J_{\mathrm{I}}$ | $-gJ_E$ |
| Background input strength | $J_{\mathrm{bg}}$ | 0.1 mV |
| Synaptic strength of dLGN→V1 | $J_{\mathrm{V1}}^{\mathrm{dLGN}}$ | 2.0 mV |
| Synaptic strength of dLGN→FFi | $J_{\mathrm{FFI}}^{\mathrm{dLGN}}$ | 2.0 mV |
| Synaptic strength of FFi→V1 | $J_{\mathrm{V1}}^{\mathrm{FFI}}$ | -1.6 mV |
| **Simulation** | | |
| Background firing rate | $\nu_{\mathrm{bg}}$ | 8 350 Hz |
| Mean luminosity of grating | $s_0$ | |
| dLGN rate response to $s_0$ | $\nu_0$ | 100 Hz |
| Stimulus orientation | $\theta$ | 0°, 15°, ... , 165° |
| Spatial frequency | $\lambda$ | 0.04, 0.08, ... cpd |
| Temporal frequency | $f$ | 3 Hz |
| Simulation time | T | 6 s |
| Contrast | $C$ | 0, 0.1, 0.3, 0.5, 0.8, 1 |

**Table 1. Table of parameters**